Journal of Archaeological Science 52 (2014) 218–241

Contents lists available at ScienceDirect

Journal of Archaeological Science

journal homepage: http://www.elsevier.com/locate/jas

In the footsteps of Pliny: tracing the sources of Garamantian carnelian from Fazzan, south-west Libya

E. Gliozzo [a, *], D.J. Mattingly [b], F. Cole [c], G. Artioli [d]

[a] Department of Earth, Environment and Physical Sciences, University of Siena, Via Laterina 8, 53100, Siena, Italy
[b] School of Archaeology and Ancient History, University of Leicester, United Kingdom
[c] UCL, Qatar
[d] Department of Geosciences, University of Padova, Italy

ARTICLE INFO

Article history:
Received 17 March 2014
Received in revised form
21 July 2014
Accepted 31 July 2014
Available online 11 August 2014

Keywords:
Carnelian
Chert
Amazonite
Fazzan (Libya)
Garamantes
Trans-Saharan trade
Beadmaking
LA-ICP-MS
XRD
Raman spectroscopy
Moganite

ABSTRACT

References in the ancient sources indicate that the Libyan desert was a source of 'carbunculi': semi-precious red stones and gemstones variously interpreted as ruby, garnet and spinel, amongst others. While gemstones are not attested in the geological strata of Fazzan (south-west Libya), a range of silica-based stones including chert, chalcedony, agate and carnelian are known to originate in this area, linked to an early civilisation known as the Garamantes. It has been long proposed that the geochemical signature and the variations in the relative proportions of quartz:moganite phases can be used to distinguish between groups of stones of different origin. The proposed methodology was tested on a number of archaeological samples from the Garamantian sites of Jarma (ancient Garama) and Saniat Jibril, in Fazzan. Fragments of chert, carnelian and amazonite found at the two sites have been identified as raw materials associated with beadmaking. Trace elemental data obtained by LA-ICP-MS were combined with mineralogical data obtained by X-ray powder diffraction and Raman spectroscopy on the same samples and a group of reference samples. The dataset has been compared with the available literature and data from other localities around the world. To this purpose a preliminary database of silica-based materials was established for provenance work. Based on the scarce data available in the literature, the importation of these stones from Eastern localities such as India may be ruled out. The measured data on archaeological samples and debitage allow us to define a reliable reference group of parameters for materials from Fazzan, which are likely to be derived from a unique geological source. The methodology should be extended and compared with cherts and carnelians from a range of Mediterranean and Sub-Saharan sites. This characterisation work is a tool of high potential utility for a new investigation of ancient contact and trade across the Trans-Saharan zone.

1. Introduction

Chert, chalcedony and other silica-based semi-precious stones (Rapp, 2002) have a prominent place in the archaeological record, as basic materials for tools and ornaments. In Northern Africa such materials are widespread both as geological and archaeological occurrences, although provenance investigations linking artefacts to geological sources are surprisingly scarce. Carnelians have been frequently recorded in Fazzan, and have been linked with Garamantian civilisation (c.500 BC – AD 700). Garamantian trade in carbuncles and other 'gems' was described by Pliny, who explicitly mentions a *Mons Giri* as the source location in the territory of the Garamantes (Pliny, *NH* 5.37: *Mons Giri in quo gemmas nasci titulus praecessit*). Carnelian is the most certain of a range of materials described by Pliny as *carbunculi* coming from a Saharan context. He specified in another passage that the Sahara was one of two main sources of carnelian for the Roman world, the other being Northern India (*NH* 37.92). He also refers to the Garamantian carbuncles being known as "Carthaginian stones" at Rome – probably a reference to the fact that Roman traders initially accessed the carnelian via Carthaginian traders? The Saharan source of carnelian only became known to Rome after acquiring her North African territory through the defeat of Carthage. Other references are less specific about the location of carnelian sources in the Sahara, suggesting that Nasamones and Aethiopes (black Africans) were also involved in procuring them (Pliny, *NH* 5.5; 37.104). Strabo likewise

* Corresponding author. Fax: +39(0)577233839.
E-mail address: gliozzo@unisi.it (E. Gliozzo).

http://dx.doi.org/10.1016/j.jas.2014.07.029
0305-4403/

referred to 'Carthaginian stones' brought from Saharan mountains and linked them to the Garamantian territory (*Geography*, 17.3.11; 17.3.19, 'the land from whence Carthaginian stones brought').

A further reference to Saharan "gems" was made by Vibius Sequester ("*Cinybs Africae, in quo plurima genera gemmarum inveniuntur…*") who incorrectly assumed that the Libyan river Cinyps (Cifani and Munzi, 2003) originated from Mons Giri. At the triumphal procession in Rome of Cornelius Balbus in 19 BC, celebrating victory over the Garamantes, a placard was carried referring to Mons Giri as the "place where precious stones were produced."

The exact locations of Mons Giri and/or carnelian sources in the Sahara are uncertain (Desanges, 1980). However, the volcanic area of the Jabal Bin Ghanima (in the basalt province of al-Haruj), the Tibesti mountains (c.300–400 km south-east of the Garamantian heartlands) or the plateau/mountains to the north of the Wadi ash-Shati (al-Hasawina and Jabal as Sawda on Fig. 1, c.200 km to the north-east of Jarma) may be potential source areas. Arab sources refer to at least one other source of carnelian, known by the desert name of Tas-an-samt, about a third of the way between Tadmakka and Ghadamis in the Adrar des Iforas (Levtzion and Hopkins, 2000; Insoll et al., 2004). There is also evidence of neolithic exploitation of carnelian for bead production in the Sahara and West Africa, though the exact source of the material is unknown (Calegari, 1993). Despite the distance of the potential raw material sources from their capital at Jarma, the Garamantes appear to have had control of quarries and transported large amounts of the raw materials there for further processing. Debitage from primary and secondary processing was recorded in excavations of Garamantian levels at Jarma (Mattingly, 2013) and at the nearby site of Saniat Jibril (Mattingly, 2010). Carnelian debitage also is a relatively common surface find at other Garamantian era settlements (Mattingly, 2003), suggesting that future excavations would enhance the emerging picture of carnelian working (Fig. 2). Although there is no potential carnelian source close to Jarma, the attested scale of primary processing carried out Garamantian sites certainly suggests a source within a few hundred km rather than further afield.

Following 19th century European travellers, Mons Giri has variously been identified with the Tassili-n-Ajjer or Tibesti mountains. In the absence of specific finds from the Wadi ash-Shati area, the most suggestive records relate to the south-east Fazzan, in the approaches to Tibesti south of Tijirhi and al-Qatrun (Fig. 1). Both the Denham and Clapperton expedition of the 1820s and that of Rohlfs in the 1860s noted numerous finds of flint, hornstone, chalcedony, and carnelian samples in this area. Konig quoted in Denham and Clapperton 1826: "Yellowish white substance intermediate between hornstone and chalcedony, in angular pieces, with cream-coloured cachalong on the surface. 'On the way from Gatrone to

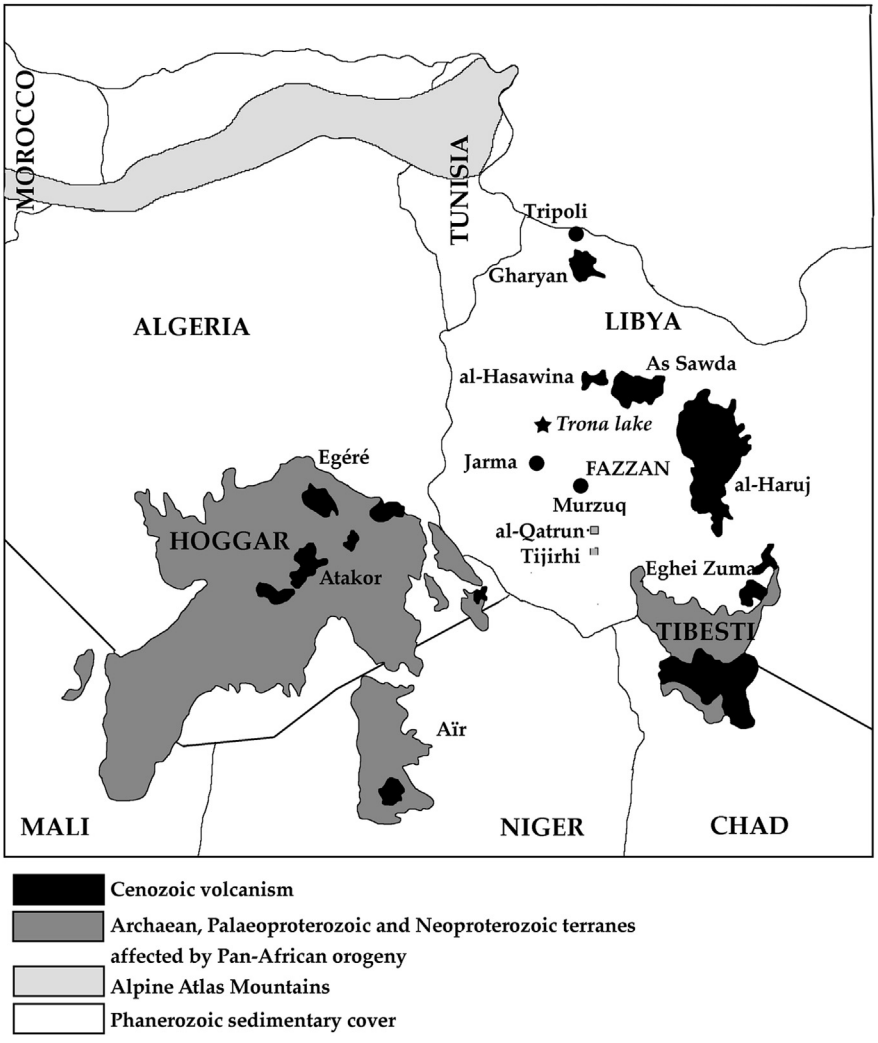

Fig. 1. Cenozoic volcanism in northern Africa and main Saharan locations mentioned in the text (after Liégeois et al., 2005).

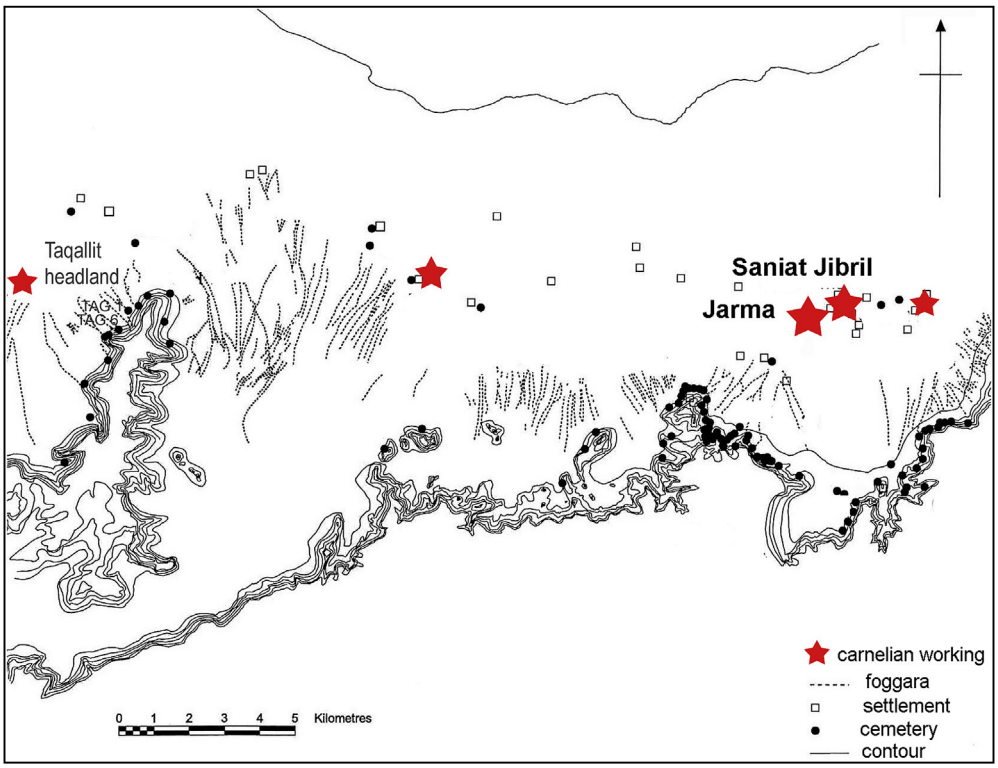

Fig. 2. Garamantian settlements with evidence of carnelian working in western Wadi al-Ajal.

Tegerhy'. Brownish-red carnelian; a fragment, with irregularly botryoidal yellowish decomposed surface. From ditto." Rohlfs (2001) describes seeing dressed stone and a column at the "well of Mechrou", two days journey to south of Tijirhi at the traditional southern limit of Fazzan, as well as evidence of semi-precious stones "Je crois plutôt que les Garamantes … avaient ici leurs carrières d'agate et de calcédoine, car on trouve encore aujourd'hui de très belles pierres vertes, jaunes et rouges" ("I think that the Garamantes had their quarries of agate and carnelian close by, for one still finds today very nice stones in green, yellow and red").

The alleged presence of other types of red gemstones variously interpreted by modern scholars as ruby, garnet or spinel (amongst others) is still much debated, but it is geologically unlikely that such precious stones originated from the region. They are virtually non-occurring in the area and, if present, it is likely that the Garmantes obtained them through long-distance trade with the Mediterranean, Nilotic, sub-Saharan or West African regions, with all of which areas they were in contact with. The specific problem of green amazonite will be briefly discussed separately. As with carnelian and red gemstones, modern myths have grown up surrounding Garamantian "emeralds" when amazonite was more likely the material referred to in the sources (Monod, 1984). A main quarry source of Saharan amazonite has been identified at Eghei Zuma in the northern Tibesti (De Michele and Piacenza, 1999).

The nature of the precious and semi-precious stones from the Sahara matters because, if we can establish distinctive geochemical signatures for different sources, these materials have the potential to inform us about ancient long-range contacts and trade across the Trans-Saharan zone (linking Lake Chad and the Mediterranean and the Nile and the Niger). Following the work performed by Insoll et al. (2004), this article undertook a broad selection of materials from Fazzan to be investigated by means of a wide range of techniques.

The possibility of characterising semi-precious stones based on micro- and crypto-crystalline silica like chert, chalcedony, agate and carnelians of different origin has been long proposed in the literature (Gotze et al., 1998) based on the relative proportion of quartz and moganite (Pretola 2001; Gliozzo et al., 2011). The work presented here was designed to test this methodology on a number of archaeological samples (beads and debitage) from the Garamantian sites of Jarma (GER001) and Saniat Jibril (GER002), located between Sabha and Awbari in Fazzan (Fig. 2) Jarma is the ancient Garamantian capital, a walled mudbrick city sited on a narrow belt of fertile land between a rocky escarpment and the sand-sea (Mattingly, 2003, 2013), while Saniat Jibril was a neighbouring village. Samples from Jarma originate from Proto-urban (400–1 BC) and Classic/Late Garamantian levels (AD 1–600). Some material came from the earliest phases of the site, buried beneath a monumental building identified as a temple (Mattingly, 2013). The site of Saniat Jibril lies c.0.5 km from Jarma. Survey produced substantial quantities of worked carnelian in the form of complete and half-finished beads and other small artefacts, rough fragments of carnelian and of a semi-translucent brown cherty debitage. A key point of the analysis reported here was to determine if the chert flakes and chippings were correctly identified as processing debris linked to carnelian working. The site also yielded green stones (tentatively identified as amazonite), metalwork, and glass beads in various stages of completion. Saniat Jibril is now interpreted as being an industrial suburb of Jarma, with a focus on bead and jewellery production in the period c.AD 100–400 (Mattingly, 2007). Both Jarma and Saniat Jibril are located in the Wadi al-Ajal, and form the hub of what was a network of routeways for trans-Saharan trade in antiquity. The aims of the work were:

a) To characterise the silica-based materials from the mineralogical and chemical points of view and to check whether the

Garamantian archaeological samples form a homogeneous group of materials;

b) To compare the Libyan materials with the available literature and data from other localities around the world, in order to establish the possibility of discriminating the African materials from other occurrences;

c) To assemble a preliminary database of silica-based materials and define the measurable discriminating parameters useful for future provenance work.

2. Materials

A set of archaeological samples, including beads, fragments and processing debitage (Table 1; Fig. 3) were selected for archaeometric investigation. The stone sample encompasses three major colour groups: red (in the web version) (16 samples), yellowish-grey (15 samples), and green stones preliminarily labelled as amazonites (6 samples). The first two groups were thought to relate to the primary processing of carnelian from a chert matrix, since this material derives from mixed deposits of chippings and partially worked material. Within each group the samples are typologically defined as beads, partially perforated chips, chips, processing debitage, flakes, and irregular fragments.

Samples originated from both survey and excavation at Old Jarma and Saniat Jibril. The material was collected in two phases of fieldwork – by Charles Daniels in the 1960s-1970s and by the Fazzan Project (director David Mattingly) in the 1990s-2000s (Mattingly, 2007, 2010, 2013). The site of Jarma was first inhabited in the early centuries BC, growing to become the Garamantian capital in the first century AD, then shrinking to a much smaller settlement in the post-Garamantian – early Islamic periods. Low-level occupation of the site continued into the 1930s, when the few remaining inhabitants were removed to nearby 'new' Jarma (Mattingly, 2013). Carnelian samples from Jarma were obtained from Proto-urban, Classic and Late Garamantian levels (400–1 BC, AD 1–400, 400–700). There is no evidence that carnelian working continued at the site in Post-Garamantian and Islamic eras. The site of Saniat Jibril was occupied between c.AD 100–400 (Mattingly, 2010). Samples were collected from a grid survey of the excavated site and a sieve survey of the 1973 excavation spoil heaps. All are considered to relate directly to the site's occupation (Mattingly, 2010).

Carnelian and chert debitage from both sites is considered to be a side-product of carnelian bead manufacture (Cole, 2013). Francis (2002) describes the reduction process of carnelian 'cobbles', in which the uneven brown stone surface is chipped away to reveal the translucent red core within. Chert and carnelian were differentiated by colour alone. At Jarma and Saniat Jibril, both materials originate from contexts or sites firmly dated to the Garamantian period and are not considered to be residual material from the prehistoric periods.

Turquoise/green stones have been indicated as amazonite. The difficulties in making field identifications of amazonite from the range of turquoise green stones used by the Garamantians (Cole, 2013; Zerboni and Vignola, 2013) has led to an over-identification of this gemstone in the literature. Alternate turquoise-coloured stones found in the region include serpentine

Table 1
Sample list and description with findsites (GER001 = Old Jarma; GER002 = Saniat Jibril).

Easy sort	Sample	Year	Site	Find#	Context	Date	Notes/codes	Description
Carnelian	1	1997	GER002	1017	010 survey unit	1st–4th century AD	–	Half finished bead
Carnelian	2A	1997	GER002	1277	001 survey unit	1st–4th century AD	–	Chip
Carnelian	2B	1997	GER002	–	–	1st–4th century AD	–	Chip
Carnelian	2C	1997	GER002	–	–	1st–4th century AD	–	Chip
Carnelian	2D	1997	GER002	–	–	1st–4th century AD	–	Chip
Carnelian	2E	1997	GER002	–	–	1st–4th century AD	–	Chip
Carnelian	3	2000	GER002	1358	019 survey unit	1st–4th century AD	–	Chip
Carnelian	4	2001	GER001	2526	G1 751	1st–4th century AD	–	Chip
Carnelian	5	2010	GER002	–	–	1st–4th century AD	mc-53	Chip, part-perforated
Carnelian	6A	2010	GER002	–	Sieve survey, point 5–6	1st–4th century AD	mc-50	Chip
Carnelian	6B	2010	GER002	–	–	1st–4th century AD	–	Chip
Carnelian	9	2010	GER002	–	–	1st–4th century AD	mc-54	Chunk
Carnelian	17A	1969	GER001.3	–	117, 200	3rd–1st century BC	–	Chip
Carnelian	18	1969	GER001.3	–	163	4th–3rd century BC	–	Bead
Carnelian	20	1969	GER001.4	–	1766	1st century BC/AD	–	Chip
Carnelian	21G	1969	GER001.4	–	206	1st century BC	–	Chip
Chert	17B	1969	GER001.3	–	117, 200	3rd–1st century BC	–	Chip
Chert	19A	1969	GER001.3	–	170	4th–3rd century BC	–	Processing debitage
Chert	19B	1969	GER001.3	–	170	4th–3rd century BC	–	Processing debitage
Chert	19C	1969	GER001.3	–	170	4th–3rd century BC	–	Processing debitage
Chert	19D	1969	GER001.3	–	170	4th–3rd century BC	–	Processing debitage
Chert	19E	1969	GER001.3	–	170	4th–3rd century BC	–	Processing debitage
Chert	19F	1969	GER001.3	–	170	4th–3rd century BC	–	Processing debitage
Chert	19G	1969	GER001.3	–	170	4th–3rd century BC	–	Processing debitage
Chert	21A	1969	GER001.4	–	206	1st century BC	–	Chip
Chert	21B	1969	GER001.4	–	206	1st century BC	–	Chip
Chert	21C	1969	GER001.4	–	206	1st century BC	–	Chip
Chert	21D	1969	GER001.4	–	206	1st century BC	–	Chip
Chert	21E	1969	GER001.4	–	206	1st century BC	–	Chip
Chert	21F	1969	GER001.4	–	206	1st century BC	–	Chip
Chert	22	1973	GER002	–	2.76	1st–4th century AD	–	Flake?
Amazonite?	12	2000	GER001	–	665	3rd–4th century AD	sf900	Chunk
Amazonite?	13	2010	GER002	–	–	1st–4th century AD	sfMC55	Broken chip, part-perforated
Amazonite?	14	2010	GER002	–	–	1st–4th century AD	sfMC58	Chunk
Amazonite?	15	2010	GER002	–	–	1st–4th century AD	sfMC59	Perforated chip
Amazonite?	16A	2001	GER001	–	896	2nd century AD	sf2402	Chip
Amazonite?	16B	2001	GER001	–	896	2nd century AD	sf2402	Chip

and aventurine. Zerboni and Vignola (2013) characterised a range of turquoise stone samples found at the Garamantian site of Fewet, Southern Libya. While they determined that four of their samples were amazonite, comparison with amazonite samples from Eghei Zuma indicated that the Fewet materials originated from a different source.

Amazonite finds at Garamantian sites have been linked by De Michele and Piacenza (1999) to a potential source in a pegmatite dyke at Eghei Zuma, in the Tibesti mountains, southern Libya; they have confirmed a geochemical match between a sample from Jarma and raw materials from that area.

In addition to the archaeological samples, a set of ten chert samples of different origin and spanning the whole known range of quartz/moganite ratio were selected for the construction of the calibration curve.

3. Experimental

3.1. Scanning electron microscopy

The major and minor element concentrations were estimated by energy dispersive spectrometry (EDS) coupled to scanning electron microscopy (SEM). The samples were carbon-coated and directly mounted on sample holders without surface polishing (i.e. non-flat geometry), therefore sacrificing the analytical accuracy for the sake of non-destructiveness. Most EDS measurements were performed in close proximity of the hole produced by the laser ablation, so to have analytical results derived from the same portion of sample. The employed instrument is a Philips XL 30 scanning electron microscope, equipped with an energy-dispersive spectrometer EDAX-DX4, working at 20 kV (Department of Earth, Environment and Physical Sciences, University of Siena). A variety of natural silicates, oxides and synthetic materials was used as primary and quality control standards. The results of the chemical analyses for major and minor elements are reported in Table 2 for carnelians and cherts and Table 6 for green samples.

3.2. Laser ablation – inductively coupled plasma – mass spectrometry

The trace element content of carnelians, cherts, and amazonites was determined by laser ablation-inductively coupled plasma-mass spectrometry (LA-ICP-MS at (CNR, Pavia, Italy). The instrument combines an ablation microbeam based on a Nd:YAG laser source (Brilliant, Quantel) operating at 266 nm (for details see Tiepolo et al., 2003), and a quadrupole ICP-MS (Drc-e, Perkin Elmer). Thirty four masses from ^{7}Li to ^{238}U were acquired; the laser was operated at 10 Hz of repetition rate, the power on the sample was

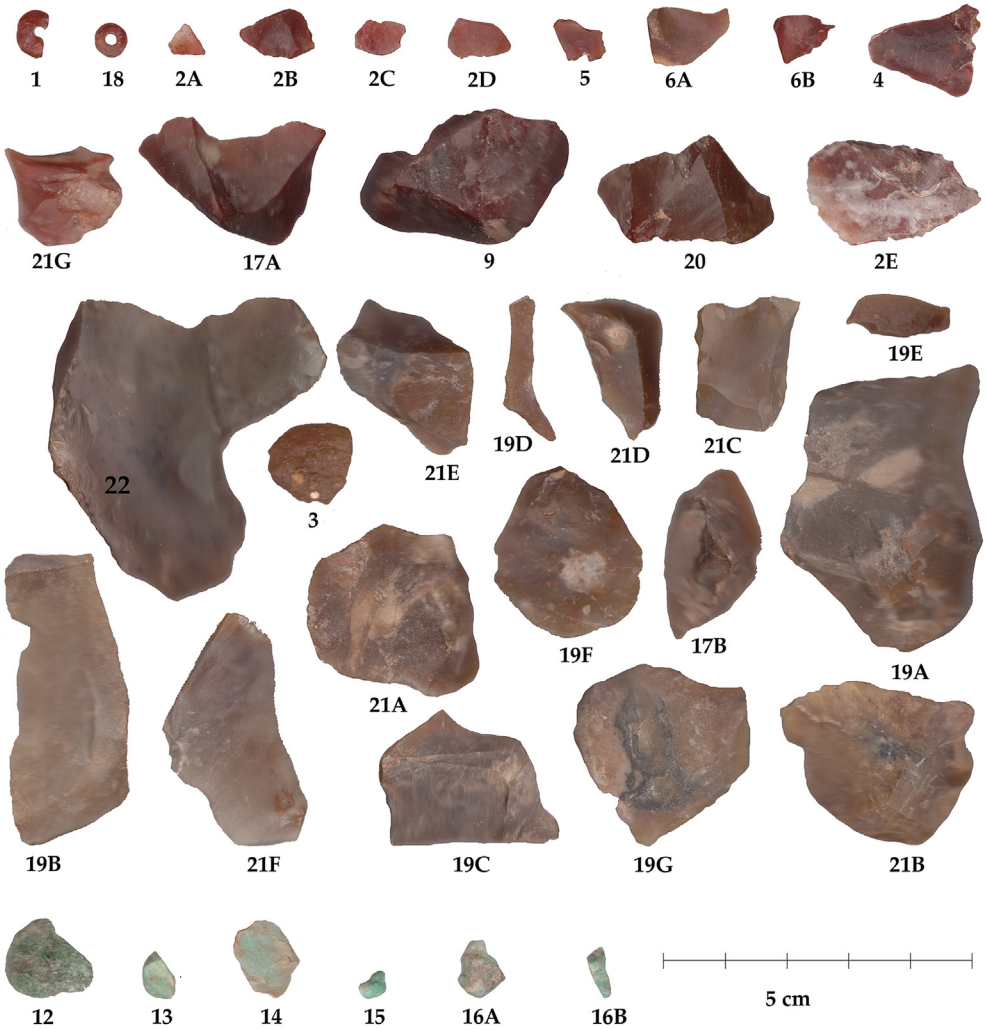

Fig. 3. The silica-based semi-precious stones from Fazzan here investigated: carnelians (1, 2A–2E, 3–5, 6A–6B, 9, 17A, 18, 20, 21G), cherts (17B, 19A–19G, 21A–21F, 22) and amazonites (12–15, 16A–16B).

Table 2
Major and minor element composition (wt %) by SEM-EDS of investigated carnelians and cherts. C stands for carnelians; H stands for cherts. [# = sample inventory no.; *a* = average; *s* = standard deviation; *mn* = minimum value; *mx* = maximum value].

# C	1		2A		2B		2C		2D		3		4		5		6A		6B		9		17A		18		20		21G		*a*	*mn*	*mx*
n = 10	*a*	*s*	*a*	*s*	*a*	*s*	*a*	*s*	*a*	*s*	*a*	*s*	*a*	*s*	*a*	*s*	*a*	*s*	*a*	*s*	*a*	*s*	*a*	*s*	*a*	*s*	*a*	*s*	*a*	*s*	*n* = 150		
Na_2O	0.2	0.0	0.1	0.1	0.2	0.2	0.1	0.1	0.1	0.1	0.1	0.1	0.2	0.1	0.1	0.1	0.0	0.1	0.2	0.3	0.2	0.1	0.2	0.2	0.2	0.2	0.4	0.1	0.1	0.1	0.2	0.0	0.4
MgO	0.2	0.1	0.3	0.0	0.1	0.0	0.1	0.1	0.2	0.1	0.8	0.2	0.3	0.3	0.2	0.2	0.2	0.3	0.3	0.3	0.3	0.1	0.1	0.5	0.3	0.2	0.4	0.1	0.1	0.0	0.3	0.1	0.8
Al_2O_3	0.8	0.1	0.5	0.1	0.5	0.2	0.8	0.3	0.4	0.5	1.4	0.8	0.7	0.6	0.5	0.4	0.8	1.0	0.5	0.1	0.4	0.0	0.3	0.5	0.5	0.3	0.6	0.2	1.0	0.8	0.6	0.3	1.4
SiO_2	97.2	0.1	97.5	0.3	97.4	0.4	98.0	1.1	97.4	3.4	96.2	1.2	98.1	0.9	98.6	0.8	98.5	1.1	98.5	1.0	98.2	0.6	98.7	0.3	98.7	1.1	97.9	1.5	97.9	0.4	97.9	96.2	98.7
K_2O	0.3	0.0	0.4	0.1	0.3	0.0	0.2	0.1	0.1	0.3	0.3	0.1	0.4	0.5	0.2	0.1	0.1	0.0	0.2	0.1	0.2	0.1	0.3	0.0	0.2	0.0	0.2	0.1	0.3	0.1	0.2	0.1	0.4
CaO	0.5	0.2	0.1	0.1	0.8	0.2	0.5	0.2	0.7	0.3	0.4	0.2	0.1	0.4	0.2	0.2	0.1	0.0	0.1	0.1	0.1	0.3	0.1	0.1	0.0	0.0	0.2	0.2	0.2	0.0	0.3	0.0	0.8
TiO_2	0.2	0.0	0.1	0.1	0.1	0.0	0.0	0.0	0.1	0.1	0.1	0.1	0.1	0.1	0.0	0.1	0.0	0.1	0.1	0.1	0.1	0.1	0.1	0.2	0.1	0.1	0.1	0.1	0.1	0.0	0.1	0.0	0.2
MnO	0.1	0.0	0.1	0.1	0.1	0.1	0.0	0.1	0.0	0.0	0.0	0.1	0.1	0.1	0.0	0.0	0.0	0.1	0.1	0.2	0.2	0.1	0.2	0.5	0.1	0.1	0.1	0.1	0.0	0.0	0.1	0.0	0.2
FeO	0.4	0.0	1.0	0.2	0.5	0.0	0.5	0.3	1.0	0.4	0.6	0.1	0.2	0.3	0.3	0.0	0.3	0.3	0.1	0.1	0.4	0.4	0.1	0.4	0.1	0.1	0.1	0.1	0.3	0.1	0.4	0.1	1.0
Tot	100		100		100		100		100		100		100		100		100		100		100		100		100		100		100				
# H	17B		19A		19B		19C		19D		19E		19F		19g		21A		21B		21C		21D		21E		21F		22		*a*	*mn*	*mx*
n = 10	*a*	*s*	*a*	*s*	*a*	*s*	*a*	*s*	*a*	*s*	*a*	*s*	*a*	*s*	*a*	*s*	*a*	*s*	*a*	*s*	*a*	*s*	*a*	*s*	*a*	*s*	*a*	*s*	*a*	*s*	*n* = 150		
Na_2O	0.1	0.1	0.3	0.2	0.3	0.3	0.2	0.1	0.1	0.2	0.2	0.3	0.3	0.3	0.3	0.2	0.2	0.1	0.4	0.1	0.2	0.2	0.1	0.1	0.1	0.1	0.2	0.1	0.0	0.0	0.2	0.0	0.4
MgO	0.1	0.3	0.4	0.4	0.3	0.2	0.4	0.1	0.1	0.5	0.4	0.4	0.4	0.2	0.5	0.4	0.3	0.2	0.1	0.1	0.4	0.3	0.3	0.2	0.1	0.0	0.2	0.1	0.1	0.0	0.3	0.1	0.5
Al_2O_3	0.3	0.2	0.7	0.4	0.6	0.1	0.6	0.1	0.6	0.3	0.9	0.6	0.7	0.7	0.9	0.6	0.6	0.6	0.8	0.0	0.9	0.8	1.0	0.8	0.6	0.0	0.7	0.4	0.5	0.2	0.7	0.3	1.0
SiO_2	99.2	0.9	97.5	0.9	97.7	1.8	98.0	0.6	98.1	1.6	97.8	1.4	97.5	2.1	97.2	1.2	98.2	1.3	97.2	1.5	97.2	1.4	97.2	1.8	97.5	2.3	98.1	0.2	98.7	0.6	97.8	97.2	99.2
K_2O	0.1	0.0	0.1	0.1	0.1	0.1	0.2	0.0	0.6	0.4	0.2	0.1	0.1	0.0	0.2	0.1	0.1	0.1	0.2	0.1	0.4	0.1	0.3	0.1	0.4	0.1	0.1	0.1	0.2	0.1	0.2	0.1	0.6
CaO	0.0	0.0	0.1	0.0	0.1	0.1	0.1	0.1	0.2	0.1	0.1	0.1	0.1	0.1	0.1	0.1	0.1	0.1	0.4	0.2	0.3	0.1	0.6	0.2	0.7	0.2	0.3	0.2	0.1	0.0	0.2	0.0	0.7
TiO_2	0.1	0.2	0.2	0.0	0.2	0.1	0.1	0.1	0.0	0.1	0.1	0.0	0.1	0.0	0.1	0.1	0.1	0.1	0.2	0.1	0.1	0.0	0.1	0.1	0.2	0.1	0.1	0.1	0.1	0.1	0.1	0.0	0.2
MnO	0.1	0.1	0.2	0.0	0.2	0.0	0.1	0.1	0.0	0.0	0.1	0.1	0.1	0.1	0.1	0.1	0.1	0.1	0.2	0.0	0.2	0.0	0.1	0.1	0.2	0.1	0.1	0.0	0.2	0.1	0.1	0.0	0.2
FeO	0.1	0.0	0.3	0.0	0.3	0.1	0.3	0.0	0.3	0.2	0.3	0.2	0.5	0.3	0.3	0.3	0.2	0.1	0.5	0.4	0.4	0.1	0.4	0.1	0.3	0.1	0.2	0.1	0.1	0.0	0.3	0.1	0.5
Tot	100		100		100		100		100		100		100		100		100		100		100		100		100		100		100				

Table 3a
The results of trace element composition (ppm) obtained on 15 carnelians by LA-ICP-MS. Three measurements were performed each sample, except for two beads (no. 1, 18) that were measured six times. [a = average; s = standard deviation]. Significant figures are to the second decimal place for major and minor elements, whereas values for trace and ultra-trace elements are significant to the third or fourth decimal place, following standardisation and experimental conditions.

Sample		1	2A	2B	2C	2D	3	4	5	6A	6B	9	17A	18	20	21G
n=		6	3	3	3	3	3	3		3	3	3	3	6	3	3
Li	a	0.81	1.14	2.50	1.11	0.56	2.71	0.79	0.61	5.50	0.81	1.68	0.79	1.17	0.60	0.93
	s	0.57	0.15	0.69	0.04	–	1.68	0.01	0.34	1.01	0.23	0.93	0.25	0.25	0.17	0.48
Be	a	1.69	1.92	0.95	1.37	1.58	0.59	0.89	0.64	1.69	1.16	4.32	1.03	7.51	0.66	1.57
	s	0.15	0.18	0.56	0.90	0.08	0.23	0.67	0.34	0.01	0.12	2.37	0.52	2.38	0.29	–
B	a	38.41	29.69	7.99	11.84	14.58	26.13	5.51	2.76	12.00	15.52	10.24	7.92	6.50	5.77	5.92
	s	5.33	6.41	0.77	1.62	1.22	12.63	0.62	1.06	10.28	1.27	5.20	0.45	2.95	0.36	2.57
Sc	a	3.72	2.24	2.77	2.67	2.50	6.36	5.14	6.03	4.70	2.65	2.10	2.61	4.35	2.63	3.39
	s	1.18	0.06	0.25	0.17	0.03	0.64	0.08	0.50	0.45	0.47	0.33	0.10	0.79	0.29	0.39
V	a	4.39	1.34	2.28	2.19	2.11	8.47	1.47	1.52	5.05	2.05	1.85	0.80	1.60	1.18	0.68
	s	2.47	0.38	1.17	0.15	0.51	3.18	0.43	0.21	3.71	1.55	1.01	0.43	0.93	0.16	0.14
Cr	a	3.84	4.33	4.32	5.63	3.73	5.99	4.94	<1.78	9.27	<5.23	5.69	4.58	7.01	<2.94	<3.71
	s	1.05	0.84	2.36	1.97	1.11	1.21	2.26	–	6.43	–	1.41	1.15	–	–	–
Co	a	0.338	0.225	0.364	0.233	0.152	1.215	0.191	0.101	0.989	<0.236	0.268	0.178	0.168	0.108	0.098
	s	0.138	0.033	0.065	0.035	0.031	0.748	0.007	0.038	0.503	–	0.163	0.075	0.067	0.055	–
Ni	a	2.01	2.08	1.77	0.98	1.82	3.02	1.92	2.16	4.66	2.28	2.22	1.44	2.88	1.73	2.05
	s	0.66	0.62	0.27	0.01	0.26	0.14	0.50	0.58	0.97	0.54	0.25	0.34	0.39	0.46	0.04
Zn	a	6.21	3.81	5.89	7.42	20.82	25.35	8.58	2.74	19.13	3.39	13.03	11.67	20.56	3.03	7.07
	s	2.38	1.97	2.63	0.99	18.96	1.63	1.39	0.18	15.91	0.46	3.27	1.14	5.55	1.49	2.28
Rb	a	1.44	1.71	2.24	0.87	0.86	4.18	0.95	0.50	10.43	0.52	2.61	1.27	1.77	0.64	0.30
	s	0.75	0.75	0.45	0.20	0.01	0.40	0.27	0.13	9.45	0.09	1.02	0.53	1.58	0.06	0.08
Sr	a	4.10	4.25	5.46	18.83	13.37	75.90	4.43	2.37	16.90	1.74	3.91	3.88	4.70	1.01	2.33
	s	0.86	0.53	0.96	5.52	2.01	60.89	1.98	0.73	12.47	0.49	0.78	1.11	2.69	0.19	0.46
Y	a	0.210	0.123	0.436	0.191	0.558	0.613	0.246	0.180	0.597	<0.191	0.273	0.242	0.223	0.066	0.044
	s	0.153	0.032	0.248	0.015	0.127	0.215	0.191	0.028	0.308	–	0.077	0.192	0.082	0.028	0.022
Zr	a	0.58	0.51	2.24	0.84	0.71	1.98	1.06	0.31	3.22	0.41	1.38	0.59	0.67	0.26	0.48
	s	0.19	0.28	0.33	0.11	0.08	0.01	0.28	0.05	0.70	0.10	0.30	0.24	0.25	0.05	0.09
Nb	a	0.120	0.169	0.300	0.069	0.040	0.465	0.194	0.078	0.886	<0.147	0.237	0.147	0.227	0.117	0.072
	s	0.099	0.036	0.139	0.000	0.015	0.024	0.111	0.037	0.581	–	0.090	0.178	0.100	0.026	0.014
Cs	a	0.0812	0.0509	0.1013	0.0356	0.0418	0.2201	0.0505	0.0216	0.3799	<0.105	0.1254	0.0346	0.1507	0.0357	0.0193
	s	0.0440	0.0106	0.0014	0.0104	0.0035	0.1216	0.0454	0.0111	0.2518	–	0.0531	0.0214	0.1390	0.0173	0.0039
Ba	a	3.59	1.53	7.39	20.00	4.17	30.53	6.67	2.68	17.54	1.15	8.15	3.47	5.40	2.05	3.16
	s	3.09	0.12	0.90	4.58	0.94	14.07	1.14	0.37	7.52	0.46	0.90	0.43	2.29	0.35	0.04
La	a	0.318	0.249	0.425	0.166	0.256	1.231	0.404	0.102	1.226	0.060	0.315	0.196	0.138	0.036	0.040
	s	0.126	0.028	0.267	0.003	0.102	0.241	0.216	0.024	0.477	0.011	0.171	0.119	0.120	0.011	0.001
Ce	a	1.012	0.578	0.669	0.700	0.724	4.296	1.036	0.375	3.780	0.269	1.268	0.424	0.446	0.139	0.130
	s	0.335	0.135	0.266	0.024	0.165	2.282	0.397	0.114	2.742	0.053	0.450	0.060	0.227	0.050	0.055
Pr	a	0.059	0.063	0.086	0.039	0.055	0.372	0.116	0.043	0.338	<0.104	0.098	0.046	0.071	0.012	0.007
	s	0.030	0.030	0.034	0.010	0.018	0.050	0.108	0.022	0.284	–	0.059	0.031	0.062	0.009	–
Nd	a	0.345	0.111	0.300	0.265	0.188	1.399	0.560	0.125	1.132	0.162	0.374	0.106	0.146	0.076	0.084
	s	0.235	0.028	0.017	0.108	0.045	0.729	0.155	0.030	0.551	–	0.235	0.032	0.149	–	0.033
Sm	a	0.103	0.089	0.066	0.025	0.137	0.225	0.090	0.060	0.214	<0.41	0.102	0.094	0.089	0.047	<0.071
	s	0.057	0.023	0.013	0.000	–	0.100	0.102	0.002	0.006	–	–	0.017	0.080	0.024	–
Eu	a	0.032	0.026	0.029	0.022	0.028	0.047	0.020	0.025	0.057	<0.150	0.025	0.020	0.014	0.027	<0.00
	s	0.034	0.008	0.031	0.015	0.003	0.001	0.014	–	0.037	–	0.008	0.015	0.000	–	–
Gd	a	0.097	0.064	0.050	<0.073	0.115	0.190	0.209	0.070	0.105	<0.30	0.067	0.063	0.047	0.042	0.025
	s	0.069	0.056	0.035	–	0.059	0.052	–	0.023	0.053	–	0.048	0.045	–	–	–
Tb	a	0.0161	0.0151	0.0103	0.0150	0.0168	0.0319	0.0068	0.0053	0.0513	<0.095	0.0198	0.0051	0.0036	0.0034	<0.0072
	s	0.0124	0.0006	0.0042	0.0031	–	0.0054	0.0012	0.0015	0.0058	–	0.0085	–	0.0001	–	–
Dy	a	0.0979	0.0571	0.0669	0.0144	0.0536	0.1720	0.0297	0.0224	0.1268	0.0706	<0.094	<0.040	0.0360	<0.026	0.0316
	s	0.0724	0.0320	0.0070	0.0000	0.0160	0.0041	0.0028	0.0073	0.0781	–	–	–	0.0308	–	–
Ho	a	0.0042	0.0167	0.0073	0.0076	0.0111	0.0311	<0.0080	0.0073	0.0228	<0.102	0.0162	0.0140	0.0088	0.0051	0.0041
	s	0.0002	–	0.0031	0.0038	0.0049	–	–	0.0022	0.0048	–	–	0.0053	0.0101	0.0022	–
Er	a	0.0236	<0.047	0.0170	0.0158	0.0664	0.0408	0.0183	0.0192	0.0617	<0.193	0.0218	–	0.0375	0.0140	0.0168
	s	0.0028	–	0.0007	0.0000	0.0035	–	0.0105	0.0142	0.0492	–	–	–	0.0316	–	–
Tm	a	0.0042	0.0090	<0.0077	0.0072	0.0114	0.0127	0.0027	0.0095	0.0189	<0.096	0.0194	0.0094	<0.028	<0.0063	0.0040
	s	<0.026	0.0069	–	0.0000	0.0006	0.0139	0.0003	0.0105	–	–	–	–	–	–	–
Yb	a	0.043	0.029	0.026	0.024	0.053	0.051	0.071	0.028	0.064	0.189	0.096	–	0.023	<0.043	0.026
	s	0.021	–	0.001	0.000	–	–	0.018	–	–	–	–	–	0.001	–	–
Lu	a	0.0230	0.0083	<0.0051	0.0039	0.0213	0.0093	0.0086	0.0023	0.0033	<0.082	0.0103	0.0053	0.0098	<0.0066	0.0042
	s	0.0111	0.0043	–	0.0000	–	0.0093	0.0032	–	–	–	0.0072	0.0003	0.0096	–	–
Hf	a	0.0452	0.0259	0.0310	0.0188	0.0216	0.0690	0.0282	0.0175	0.0855	<0.169	0.0834	0.0389	0.0189	<0.033	<0.00
	s	0.0210	0.0030	0.0132	0.0000	–	–	0.0175	0.0075	–	–	–	0.0169	–	–	–
Ta	a	0.0103	0.0159	0.0103	0.0038	0.0080	0.0168	0.0073	0.0034	0.0422	<0.079	0.0265	0.0153	<0.031	0.0053	0.0083
	s	0.0022	0.0117	0.0084	0.0000	0.0054	0.0019	0.0067	0.0017	0.0238	–	0.0092	0.0143	–	0.0027	–
Pb	a	2.24	0.71	0.55	0.23	0.70	0.80	0.70	0.17	2.59	0.34	0.75	0.75	3.39	0.67	4.38
	s	1.43	0.27	0.03	0.02	0.49	0.36	0.23	0.02	0.15	0.08	0.29	0.32	0.52	0.14	1.45
Th	a	0.059	0.079	0.097	0.042	0.048	0.209	0.124	0.033	0.312	0.110	0.113	0.054	0.024	0.031	0.016
	s	0.048	0.029	0.036	0.000	0.026	0.032	0.057	0.013	0.155	0.023	0.033	0.045	0.009	0.005	0.003
U	a	5.04	4.90	1.80	2.58	4.38	1.25	1.55	1.17	1.39	2.68	2.52	2.82	2.39	1.60	2.22
	s	1.05	0.45	0.12	0.03	0.10	0.22	0.01	0.02	0.42	1.51	0.20	0.19	0.21	0.04	0.01

Table 3b
The results for trace elements composition (ppm) obtained on 13 cherts by LA-ICP-MS. Three measurements were performed each sample. [*a* = average; *s* = standard deviation]. Significant figures are to the second decimal place for major and minor elements, whereas values for trace and ultra-trace elements are significant to the third or fourth decimal place, following standardisation and experimental conditions.

Sample		17B	19B	19C	19D	19E	19F	21A	21B	21C	21D	21E	21F	22
n=		3	3	3	3	3	3	3	3	3	3	3	3	3
Li	*a*	1.91	31.72	6.69	2.51	5.12	3.39	3.44	2.43	1.20	1.35	5.70	1.60	2.08
	s	0.19	1.54	1.55	0.29	1.09	0.46	0.11	1.51	0.54	0.78	1.85	0.67	0.39
Be	*a*	1.33	1.10	2.31	1.34	0.98	0.89	0.47	<1.76	<2.13	0.58	0.98	0.79	<1.58
	s	1.25	–	–	–	–	0.49	0.19	–	–	–	0.08	0.33	–
B	*a*	7.23	74.63	21.85	17.23	15.20	7.63	5.88	6.83	5.61	6.73	6.87	4.80	11.15
	s	0.64	19.30	2.78	4.44	7.20	0.71	1.62	3.05	1.29	2.88	1.81	1.06	1.67
Sc	*a*	2.39	4.33	2.66	2.65	2.49	2.85	3.45	2.87	2.11	3.16	2.85	2.87	4.18
	s	0.29	0.14	0.43	0.25	0.35	0.19	0.35	0.26	0.06	0.45	0.57	0.21	0.68
V	*a*	2.06	48.92	10.72	4.94	1.30	3.14	1.02	1.87	0.90	0.59	4.95	2.02	6.95
	s	0.35	0.26	1.69	3.21	0.26	1.63	0.30	1.46	0.46	0.04	2.84	0.37	0.38
Cr	*a*	4.73	45.95	14.18	7.80	<2.63	<2.26	<2.23	4.42	7.36	3.96	3.86	4.59	<3.15
	s	–	10.58	2.74	–	–	–	–	–	–	–	1.18	–	–
Co	*a*	0.416	10.149	1.732	0.600	0.355	0.739	0.477	0.649	0.126	0.195	1.256	0.278	0.283
	s	0.049	1.793	0.439	0.034	0.013	0.068	0.211	0.502	0.055	0.071	0.161	0.066	0.082
Ni	*a*	2.85	22.38	5.70	3.02	2.17	2.12	2.66	1.69	2.01	2.34	3.37	1.49	2.54
	s	0.63	1.14	0.83	0.27	0.96	1.02	0.43	1.14	0.40	0.19	1.43	0.55	0.39
Zn	*a*	17.81	160.51	29.48	17.17	3.25	7.99	3.19	5.57	7.81	8.11	28.24	14.15	18.12
	s	1.99	39.91	7.59	0.24	0.17	2.34	0.86	2.12	3.64	2.03	1.18	2.78	8.25
Rb	*a*	2.94	82.35	16.11	5.04	2.77	2.56	2.06	1.56	1.16	1.24	5.69	2.65	3.17
	s	1.45	5.06	4.70	0.36	0.52	0.36	0.14	0.67	0.18	0.39	4.51	0.49	0.34
Sr	*a*	9.50	100.33	23.23	6.47	6.06	2.48	2.16	9.17	2.48	3.25	8.45	3.44	14.47
	s	2.60	1.33	4.76	0.90	0.94	0.78	0.85	5.72	0.87	0.90	0.59	0.60	0.04
Y	*a*	0.171	1.914	0.589	0.108	0.110	0.171	0.076	0.197	0.066	0.099	0.143	0.203	5.865
	s	0.069	0.516	0.113	0.018	0.012	0.077	0.014	0.074	0.018	0.051	0.111	0.051	1.233
Zr	*a*	1.79	8.32	2.58	0.86	0.72	2.80	1.64	3.99	1.46	1.11	1.84	0.99	2.63
	s	0.20	2.36	0.42	0.10	0.06	0.97	0.22	0.18	0.60	0.16	0.75	0.23	1.09
Nb	*a*	0.320	6.389	1.136	0.323	0.151	0.327	0.128	0.353	0.138	0.149	0.343	0.184	0.317
	s	0.031	1.584	0.246	0.045	0.002	0.036	0.026	0.121	0.057	0.053	0.271	0.040	0.044
Cs	*a*	0.2731	3.0886	0.8742	0.1976	0.1186	0.0797	0.0846	0.0746	0.0507	0.0524	0.3247	0.1060	0.1600
	s	0.1758	0.4326	0.1534	0.0792	0.0028	0.0209	0.0042	0.0305	0.0133	0.0380	0.2306	0.0040	0.0458
Ba	*a*	9.77	59.46	39.27	6.28	11.61	15.60	8.23	6.40	3.89	3.47	12.35	6.88	11.98
	s	1.30	9.78	26.42	0.02	6.12	0.54	0.60	–	1.69	0.17	1.14	1.96	9.70
La	*a*	0.392	7.845	1.534	3.039	0.191	0.219	0.078	0.207	0.165	0.920	0.749	0.506	3.219
	s	0.184	1.786	0.056	3.183	0.082	0.041	0.058	0.115	0.086	0.033	0.948	0.265	0.423
Ce	*a*	2.512	27.906	8.180	4.039	0.515	0.491	0.265	0.722	0.495	0.479	1.803	1.468	2.475
	s	0.416	1.116	2.960	3.310	0.242	0.231	0.149	0.389	0.440	0.118	1.031	0.650	0.263
Pr	*a*	0.086	2.171	0.494	0.845	0.039	0.049	0.026	0.036	0.026	0.055	0.105	0.106	0.650
	s	0.028	0.195	0.307	0.710	0.003	0.004	0.022	0.017	0.009	0.050	0.088	0.032	0.149
Nd	*a*	0.999	6.266	1.242	1.404	0.182	0.150	0.075	0.212	0.127	0.193	0.306	0.896	2.696
	s	1.144	2.037	0.217	0.914	0.092	0.082	0.083	0.162	0.044	0.031	0.232	1.147	0.937
Sm	*a*	0.139	1.436	0.395	0.338	0.046	0.031	0.020	0.048	0.067	0.057	0.179	0.091	0.637
	s	–	0.314	0.127	0.010	0.046	0.003	–	0.019	0.024	–	–	0.084	0.142
Eu	*a*	0.059	0.419	0.051	0.041	0.017	<0.0155	0.005	0.018	0.032	0.013	0.022	0.074	0.174
	s	0.032	0.133	0.021	0.018	0.001	–	0.000	–	0.006	0.006	0.023	–	0.054
Gd	*a*	<0.077	1.401	0.133	0.412	0.124	0.031	0.017	<0.092	0.043	0.027	0.055	0.063	0.676
	s	–	0.447	0.021	0.351	–	0.003	0.000	–	0.006	0.001	0.054	0.064	0.156
Tb	*a*	0.0083	0.1307	0.0322	0.0153	<0.0071	0.0164	0.0083	<0.0141	0.0129	0.0042	0.0073	0.0043	0.1321
	s	0.0038	0.0370	0.0076	0.0094	–	0.0047	0.0077	–	0.0079	0.0001	0.0061	–	0.0190
Dy	*a*	0.0701	0.7450	0.3484	0.0203	0.0672	0.0290	0.0145	0.0619	0.0295	0.0363	0.0501	0.0508	0.7953
	s	0.0467	0.1465	0.2827	0.0007	–	0.0160	0.0057	–	–	–	0.0531	0.0352	0.1748
Ho	*a*	0.0138	0.1105	0.0486	0.0052	0.0146	0.0092	0.0065	<0.00	0.0062	0.0130	0.0055	0.0138	0.2073
	s	0.0071	0.0112	0.0236	–	0.0075	–	0.0030	–	–	–	0.0024	0.0024	0.0099
Er	*a*	0.0581	1.4876	0.0727	0.0528	<0.031	0.0202	0.0125	0.0442	0.0275	0.0280	0.0384	0.0545	0.6443
	s	–	1.5665	0.0105	0.0546	–	0.0021	–	–	–	0.0118	–	–	0.0444
Tm	*a*	0.0060	0.0246	<0.0211	<0.0103	0.0028	<0.00	<0.00	0.0050	0.0062	0.0042	0.0088	<0.0082	0.0692
	s	0.0027	0.0210	–	–	–	–	–	–	–	–	0.0038	–	0.0233
Yb	*a*	0.044	0.343	0.042	0.098	0.045	<0.00	<0.033	0.030	0.045	<0.081	0.060	0.027	0.514
	s	0.023	0.157	–	–	0.037	–	–	–	0.006	–	0.002	0.002	0.226
Lu	*a*	0.0045	0.0186	0.0115	0.0115	<0.00	0.0077	0.0059	<0.0187	<0.0254	<0.0075	0.0062	0.0090	0.0912
	s	–	0.0114	0.0069	–	–	0.0042	0.0003	–	–	–	–	0.0062	0.0148
Hf	*a*	0.0230	0.1396	<0.00	0.1070	0.0395	0.0487	0.0421	0.0746	<0.086	0.0226	0.0504	0.0565	0.0434
	s	–	0.0258	–	–	–	0.0313	0.0189	–	–	–	0.0313	0.0477	0.0317
Ta	*a*	0.0134	0.1416	0.0419	0.0137	0.0182	0.0104	0.0095	<0.0107	0.0095	0.0046	0.0234	0.0158	0.0042
	s	0.0043	0.0049	0.0220	0.0076	0.0085	0.0049	0.0034	–	0.0054	–	0.0148	0.0024	0.0001
Pb	*a*	2.57	<0.03	17.88	4.05	1.19	1.24	0.63	1.16	1.28	2.19	5.21	1.30	10.09
	s	0.64	–	3.73	2.58	0.18	0.53	0.25	0.30	0.85	0.65	1.11	0.11	1.48
Th	*a*	0.092	1.293	0.341	0.122	0.056	0.127	0.088	0.090	0.072	0.060	0.127	0.181	0.152
	s	0.023	0.237	0.056	0.029	0.031	0.000	0.089	0.051	0.041	0.025	0.068	0.044	0.060
U	*a*	2.54	2.69	1.73	2.16	1.17	1.49	1.03	1.30	1.46	1.84	1.48	1.66	0.33
	s	0.18	0.31	0.23	0.06	0.39	0.09	0.09	0.01	0.56	0.15	0.08	0.12	0.08

1.5 mW and spot size was set at 40 μm. Accuracy was assessed on the USGS BCR-2 reference glass (analysed as an unknown in each analytical run) and was better than 20% at the sub ppm level. Data reduction was carried out with the software package GLITTER (van Achterbergh et al., 2001) and using NIST SRM 610 and ^{29}Si as external and internal standards, respectively.

The results of the chemical analyses for trace elements are reported in Table 3 for carnelians and cherts and Table 7 for green samples.

3.3. Micro-Raman spectroscopy

The identification of the mineral species and the quantification of the quartz/moganite ratio were performed by micro-Raman spectroscopy, using a Jobin-Ivon Ltd confocal Labram multichannel spectrometer, equipped with Ar ion (λ = 514.5 nm^{-1}) excitation source, at powers ~2.0 mW at the object surface (Department of Earth, Environment and Physical Sciences, University of Siena). The laser light was focused through the objectives (×10, ×20 or ×50) of a Leica microscope, in conjunction with a micro-camera allowing perfect focussing of the laser. A holographic notch filter is used as a Rayleigh filter, in order to direct the Raman-scattered light onto a Peltier-cooled charge-coupled device (CCD) detector, operating at a temperature of −65 °C. The spectrometer was wave number calibrated using the standard Raman band positions of both the neon lamp and diamond. Bands are reported to within an uncertainty of ±2 cm^{-1}. The positioning was controlled by a manual micrometric stage and repeated analyses at different sample orientations were measured to decrease polarisation effects.

Table 4
Quartz/moganite mass ratios obtained by micro-Raman spectroscopy and full profile analysis of XRPD data. Raman band integral ratio (R_I), normalized to quartz (Qtz) and moganite ratio %. [n indicates the number of measurements performed on different spots of the same sample. Samples are listed with increasing moganite content. Standard deviations for Rietveld-derived phase quantities are mainly dominated by counting statistics and peak overlap, and they are of the order of 1–2 × 10^{-3} (Toraya 2000); the actual uncertainties due to sample preparation and instrumental reproducibility is of the order of 1–2 × 10^{-1}.

Sample#	Material	Raman spectroscopy					X-ray diffraction	
		n=	R_I I(466)/I(504)	Qtz %	Moganite %	sd	Qtz %	Moganite %
2e	Carnelian	5	25.8	96.2	3.8	1.2	–	
6a	Carnelian	5	22.5	95.7	4.3	0.5	–	
21g	Carnelian	6	17.4	94.6	5.4	0.3	–	
2b	Carnelian	7	16.8	94.2	5.8	1.3	–	
17b	Chert	5	15.9	93.9	6.1	1.4	–	
19f	Chert	5	16.0	93.7	6.3	1.6	–	
4	Carnelian	6	11.6	91.9	8.1	2.6	–	
21a	Chert	5	11.5	91.8	8.2	1.4	–	
21f	Chert	6	11.9	91.8	8.2	2.1	–	
21b	Chert	5	11.5	91.4	8.6	2.1	–	
19g	Chert	5	10.5	91.3	8.7	0.8	–	
21e	Chert	6	10.8	91.2	8.8	1.8	–	
18	Carnelian	6	10.3	90.7	9.3	1.7	–	
9	Carnelian	6	9.2	90.2	9.8	0.8	–	
20	Carnelian	5	8.9	89.7	10.3	1.6	–	
19e	Chert	5	8.4	89.4	10.6	0.6	–	
21d	Chert	6	8.2	89.1	10.9	0.6	–	
2c	Carnelian	6	8.1	89.0	11.0	0.6	–	
19d	Chert	5	8.1	88.9	11.1	0.9	–	
19c	Chert	5	8.3	88.8	11.2	2.4	–	
19a	Chert	5	8.1	88.6	11.4	2.0	–	
19b	Chert	5	7.8	88.5	11.5	1.0	–	
21c	Chert	6	7.2	87.7	12.3	0.6	–	
17a	Carnelian	5	6.8	87.1	12.9	1.1	–	
1	Carnelian	6	6.6	86.4	13.6	2.6	–	
5	Carnelian	5	6.2	86.0	14.0	1.0	–	
2a	Carnelian	5	5.7	84.8	15.2	2.7	–	
6b	Carnelian	5	5.7	81.4	18.6	2.3	–	
2d	Carnelian	6	4.0	79.8	20.2	1.3	–	
22	Chert	6	4.2	83.9	16.1	5.9	81.5	18.5
3	Carnelian	6	1.2	55.5	53.5	1.2	59.0	41.0
9	STD	3	24.8	96.0	4.0	0.9	97.2	2.8
1	STD	3	12.5	91.6	8.4	0.1	92.3	7.7
7	STD	3	11.8	92.1	7.9	0.8	91.6	8.4
3	STD	3	12.5	92.6	7.4	0.6	93.0	7.0
4	STD	3	9.3	90.0	10.0	2.3	92.1	7.9
10	STD	3	9.8	90.6	9.4	1.5	91.6	8.4
8	STD	3	7.5	88.0	12.0	2.6	87.8	12.2

Table 5
Descriptive statistics for 51 elements measured by the Authors for a total of 1180 entries. In the first column the number of "valid entries" has been provided for each element, in order to make immediately appreciable which elements are better used for comparison. In the following columns, the maximum, average and standard deviation value have been further provided for each given element. The elements are listed based on descending values of "Valid entries". The* indicates the elements (in bold) analysed in the present research. Statistiche descrittive.

	Valid entries	Maximum value	Average value	Standard deviation
Sm*	1036	740.0	4.12	41.03
La*	1035	3500.0	18.68	134.80
Ce*	1006	3700.0	30.13	195.44
Eu*	996	240.0	0.88	8.96
Yb*	993	1000.0	3.43	46.08
Lu*	948	170.0	0.59	7.82
Th*	887	2288.1	86.36	186.14
Tb*	869	180.0	0.97	10.77
Nd*	866	3400.0	20.71	184.75
Rb*	859	2000.0	37.73	105.07
Ba*	859	31208.0	517.58	2389.89
Sr*	851	6300.0	79.53	397.64
U*	846	1460.0	7.98	65.47
Cr*	838	1900.0	48.76	134.48
Dy*	826	1300.0	6.10	71.76
Co*	798	190.9	2.50	8.63
Sc*	780	168.9	17.05	19.13
V*	766	2200.0	27.47	110.12
Gd*	760	840.0	6.41	56.18
Cs*	749	526.8	2.61	20.92
Mn*	739	80800.0	291.82	3027.10
Ho*	738	330.0	1.55	18.19
Pr*	737	850.0	5.84	44.02
Zn*	733	5745.6	36.08	236.55
Er*	733	1050.0	4.56	56.61
Zr*	725	79351.7	159.89	2950.51
As	723	2400.0	16.03	105.51
Tm*	716	7.2	0.15	0.43
Ni*	713	4600.0	40.43	181.09
Y*	706	10000.0	22.88	376.67
Hf*	688	1140.9	2.89	43.68
Cu	680	7139.7	30.33	301.18
Sb	654	260.0	9.79	31.76
Pb*	642	10499.6	32.58	418.59
Ta*	609	42.7	0.50	2.40
Nb*	564	2454.5	11.68	106.92
Cd	503	830.0	3.05	38.03
Li*	493	361.5	27.64	37.50
Ag	486	62.8	0.87	3.68
Mo	476	52.0	1.50	4.07
Au	460	1759.0	67.31	231.87
Ge	433	28.4	2.36	2.64
Sn	430	1020.4	4.19	49.27
Be*	426	25.2	1.48	2.25
Ga	422	1086.6	18.53	61.41
W	419	102.0	4.77	13.17
Tl	397	170.0	0.97	8.77
Bi	394	58.7	1.17	3.27
B*	127	650.0	52.25	87.98
Hg	25	0.3	0.04	0.05
Se	9	0.4	0.10	0.12

As discussed in the literature (Götze et al., 1998; Schmidt et al., 2013c) the determination of the quartz/moganite ratio is essentially based on the integrated intensity ratios of the main symmetric stretching-bending vibrations of α-quartz (466 cm^{-1}) and moganite (504 cm^{-1}) (Fig. 4). The spectroscopic measurements, especially when performed on unground solid samples, present several severe limitations: a) different optical transparencies may induce different recorded intensities in samples with similar mineralogical composition; b) preferred orientation in the crystals may significantly affect the Raman-band intensities; c) the compositional heterogeneity of the sample may affect the signal recorded with the microbeam. These problems are partially controlled by repeated measurements on different spots and on different directions in the samples, however for the reasons listed above the resulting values must be intended as semi-quantitative estimates and they should be taken with caution. Therefore as an independent check on the mineral content, the peak intensity values resulting from Raman measurements reported in Table 4 have been calibrated and compared with the results from powder diffraction for a set of standard samples (see below).

3.4. X-ray diffraction

The independent assessment of the quartz/moganite ratio was obtained by full profile refinement of the intensity profiles measured by X-ray powder diffraction (XRPD). The XRPD data were collected on a set of standard reference samples (STD 1 - STD 10) and on two archaeological samples (3 and 22) using the flat plate powder mounting in Bragg-Brentano configuration. A MPD X'Pert goniometer was employed for data collection in the 10–80 °2θ range, equipped with a X'Celerator detector and Cu K radiation (Department of Geosciences, University of Padova). Full profile refinements were carried out using the GSAS software (Larson and Von Dreele, 1994). The refinement strategy included the structure model of moganite proposed by Miehe and Graetsch (1992), and

Table 6
SEM-EDS on green gemstones. The Cr-bearing phyllosilicate has been analysed in gemstone no.12. The measurements provided for feldspars represent the average values of 28 and 22 measurements complessively obtained on samples 13–15 and 16A–B. Structural formula on the basis of 22 or 8 oxygens [a = average; s = standard deviation; mn = minimum].

	Cr-bearing phyllosilicate		K-feldspar		Plagioclase	
	a (n = 8)	s	a (n = 28)	s	a (n = 22)	s
Na_2O	1.10	0.61	1.18	0.62	9.84	2.02
MgO	1.35	0.46	1.53	0.84	1.06	0.45
Al_2O_3	33.28	0.96	18.23	0.90	17.90	3.14
SiO_2	47.24	2.36	63.13	1.92	70.25	4.73
K_2O	11.80	2.97	14.12	1.00	0.31	0.14
CaO	0.22	0.07	0.62	1.41	0.18	0.08
TiO_2	1.30	0.37	0.22	0.11	0.11	0.04
Cr_2O_3	2.83	0.54	0.21	0.17	0.09	0.09
MnO	0.06	0.27	0.00	0.00	0.06	0.23
FeO	0.86	0.61	0.77	0.50	0.26	0.23
Total	100		100		100	
Na	0.276		0.168		1.351	
Mg	0.260		0.106		0.068	
Al	5.070		0.995		0.917	
Si	6.107		2.923		3.052	
K	1.946		0.834		0.017	
Ca	0.030		0.031		0.008	
Ti	0.126		0.008		0.003	
Cr	0.289		0.008		0.003	
Mn	0.000		0.000		0.000	
Fe	0.093		0.030		0.009	
Oxygen	22		8		8	

Table 7
The results of trace element composition (wt %) obtained on 6 green stones by LA-ICP-MS. Three measurements were performed each sample. [a = average; s = standard deviation].

Sample		12	13	14	15	16A	16B
n=		3	3	3	3	3	3
Li	a	6.05	5.93	0.64	13.30	18.84	48.45
	s	2.91	7.52	0.12	12.34	14.97	67.15
Be	a	0.66	8.32	11.31	7.03	4.99	7.36
	s	0.13	3.20	2.57	1.75	6.57	5.63
B	a	38.27	3.32	6.31	9.87	9.80	15.23
	s	37.65	1.21	2.77	5.54	7.48	12.69
Sc	a	12.66	1.53	2.20	1.64	1.74	2.03
	s	12.54	0.18	0.21	0.36	0.21	0.05
V	a	185.78	1.07	0.92	3.65	3.55	2.53
	s	228.05	0.79	0.58	3.98	2.93	0.48
Cr	a	4255.78	–	2.50	3.33	4.13	2.42
	s	5311.01	–	–	0.62	2.30	–
Co	a	14.435	0.283	0.112	0.823	0.597	0.568
	s	16.937	0.052	0.056	0.821	0.558	0.206
Ni	a	67.26	0.57	0.42	1.98	1.59	1.17
	s	79.48	0.48	0.43	2.11	0.62	0.60
Zn	a	71.54	6.58	4.69	16.86	24.73	16.25
	s	67.95	4.72	1.39	16.34	13.39	17.82
Rb	a	48.74	1767.91	2255.43	6197.97	6997.68	6.661.46
	s	55.09	310.95	276.86	1811.95	1170.14	373.25
Sr	a	108.59	6.52	5.5	46.56	31.25	21.03
	s	76.54	2.68	1.6	43.35	19.40	5.27
Y	a	0.259	0.165	0.065	0.469	0.264	0.141
	s	0.206	0.115	0.018	0.180	0.156	0.096
Zr	a	1.20	0.39	0.21	2.34	1.30	0.94
	s	1.11	0.20	0.02	1.59	0.32	0.61
Nb	a	0.770	0.097	0.081	0.646	0.338	0.505
	s	0.724	0.034	0.025	0.613	0.059	0.211
Cs	a	0.7620	26.0131	27.7931	171.0050	114.6850	154.8952
	s	0.3965	3.7000	3.7719	58.2397	4.1366	14.7332
Ba	a	68.69	7.13	6.88	31.09	7.91	244.34
	s	79.07	3.25	0.57	38.51	3.83	412.08
La	a	0.761	0.381	0.125	2.573	0.844	0.379
	s	0.552	0.172	0.008	3.757	0.576	0.248
Ce	a	4.012	0.836	0.334	3.439	2.460	1.444
	s	2.161	0.414	0.091	3.569	2.094	0.220
Pr	a	0.233	0.089	0.020	0.776	0.075	0.158
	s	0.167	0.066	0.008	1.188	0.016	0.106
Nd	a	0.909	0.311	0.072	0.841	0.336	0.824
	s	0.723	0.229	0.022	0.944	0.101	0.578
Sm	a	0.236	0.043	0.034	0.123	0.103	0.119
	s	0.036	0.039	0.001	0.105	0.071	0.042
Eu	a	0.100	0.048	0.018	0.054	0.026	0.035
	s	0.078	0.007	0.008	0.069	0.001	0.020
Gd	a	0.131	0.059	0.016	0.113	0.083	0.039
	s	0.065	0.057	–	0.103	0.004	0.035
Tb	a	0.0111	0.0155	−0.0051	0.0164	0.0168	0.0154
	s	0.0035	0.0008	0.0026	0.0040	0.0086	0.0058
Dy	a	0.0561	0.0871	0.0307	0.1530	0.1525	0.1126
	s	0.0092	0.0649	0.0105	0.0484	0.1124	0.1426
Ho	a	0.0208	0.0180	0	0.0281	0.0125	0.0086
	s	–	–	–	0.0031	0.0045	0.0003
Er	a	0.0526	0.5450	0.0166	0.1420	0.1030	0.0425
	s	0.0014	0.7524	0.0079	0.0791	–	0.0106
Tm	a	0.0138	0.0100	0.0024	0.0285	0.0077	0.0068
	s	0.0058	–	0.0001	0.0184	–	0.0053
Yb	a	0	0.040	0.016	0.264	0.056	0.103
	s	–	0.030	–	0.260	0.005	0.115
Lu	a	0	0.0162	0	0.0423	0.0057	0.0044
	s	–	–	–	0.0570	0.0041	0.0022
Hf	a	0.0831	0.0203	0.0273	0.2367	0.1690	0.9005
	s	–	0.0101	0.0193	0.2618	–	0.3825
Ta	a	0.0307	0.0405	0.0285	0.2830	0.0545	0.2533
	s	0.0250	0.0195	0.0206	0.3403	0.0305	0.1685
Pb	a	12.13	443.38	475.20	756.53	358.30	651.16
	s	12.54	118.39	60.51	255.90	119.95	116.39
Th	a	0.137	0.059	0.056	0.143	0.147	0.097
	s	0.089	0.047	0.033	0.172	0.153	0.088
U	a	0.31	0.03	0.02	0.19	0.17	0.16
	s	0.23	0.01	0.01	0.24	0.07	0.08

assuming the profile shape and lattice parameters of moganite refined on sample 3, which contains the maximum amount of the phase among the available samples.

The results of the quantitative estimation of the two phases following the Rietveld method are reported in Table 4.

4. Results and discussion

4.1. The Garamantian carnelians and cherts from Fazzan

The putative carnelians and cherts defined on macroscopic characteristics show rather similar chemical composition in terms of major and minor element contents (Table 2). The main constituent (SiO_2) shows mean values of 97.9 wt% in carnelians and 97.8 wt% in cherts. A modest difference was also found among a few minor elements: TiO_2 and MnO mean values are slightly larger in cherts than in carnelians; Al_2O_3 values are relatively higher in carnelian sample no. 3. CaO contents are always below 1 wt% in both carnelians and cherts; despite the variation that may be encountered, the average and the variability between maximum and minimum values are comparable. Iron contents vary between 0.1 and 1.0 wt% in carnelians and between 0.1 and 0.5 wt% in cherts, however, the average values determined per group are rather similar (0.4 and 0.3 wt% respectively). This suggests a common geological origin for the two main groups of material and that the archaeological interpretation that associated the chert debitage with extraction and working of carnelian is correct.

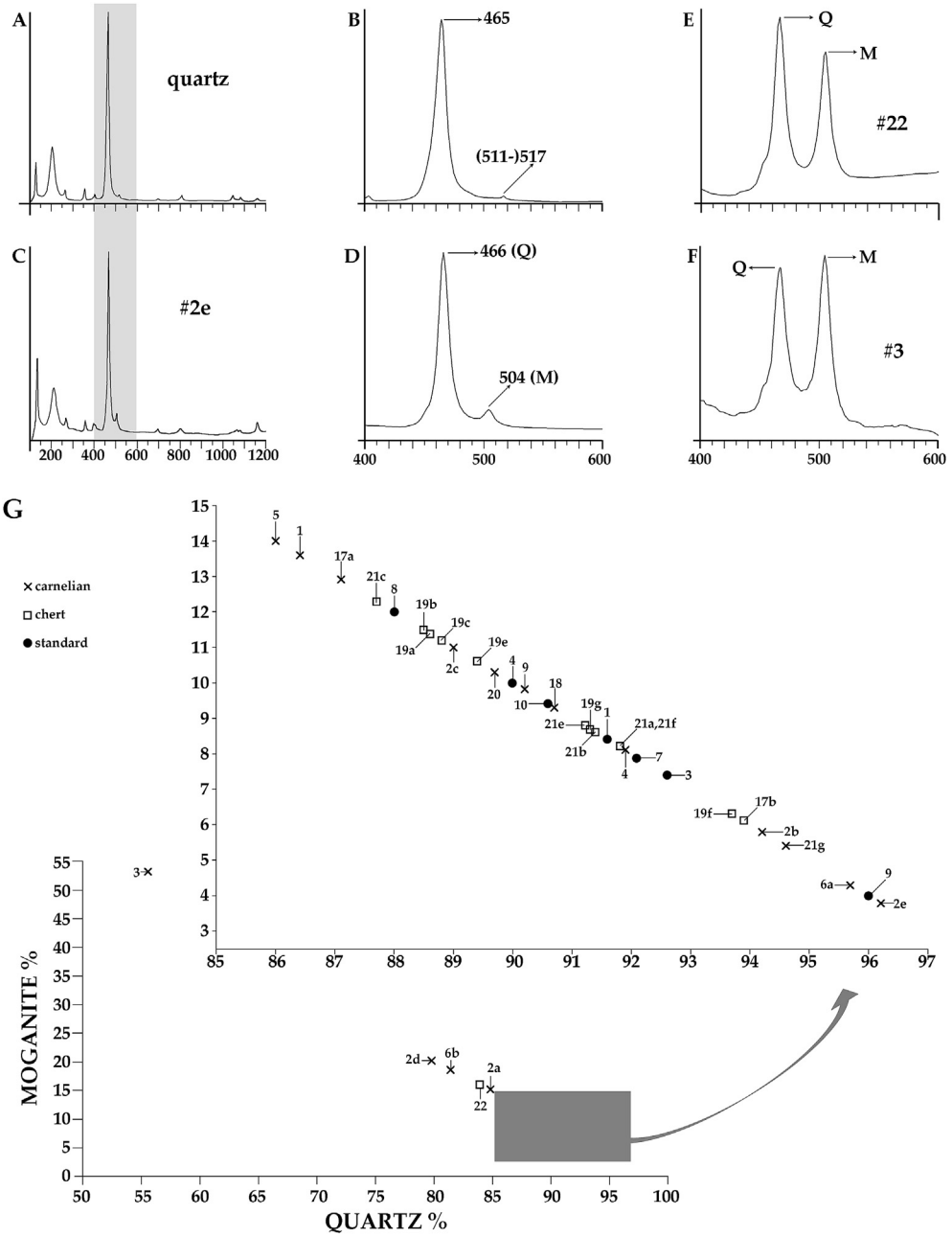

Fig. 4. Raman spectra: A–B) quartz (RUFF ID #X080015); C–D) sample 2e; E) sample 22; F) sample 3. Q stands for quartz; M stands for moganite. Note that B and D are magnifications of A and C. G) Binary diagram showing quartz and moganite ratio % in archaeological samples and reference materials used as standards.

Taking into account the relatively large standard deviations of the trace element contents for both carnelians and cherts (Table 3), no clear distinction can be observed between the two groups. As a matter of fact the concentration pattern across the REE (Fig. 5) is very similar for all samples, showing maxima for Ce and Nd, except that the chert sample 19B shows concentration values larger by a factor of 3–4 with respect to carnelian samples 3 and 6A and chert sample 19C, and by a factor of 10–12 with respect to the other carnelian or chert samples. The positive Ce and Nd anomalies may indicate a different origin of these 4 samples (3, 6A, 19B, and 19C); for instance, marked enrichments in Ce and Nd generally occur in rocks late in a magmatic series, such as peralkaline granite.

With respect to all other samples it should be noted that they form a very homogeneous group from the chemical point of view.

Concerning the mineral phases, the Raman spectra of all the archaeological samples show the distinct peak of moganite at 504 cm^{-1} (as shown in Fig. 4C and D for sample 2e). The vast majority of Libyan carnelians and cherts plot in the lower-right region of the moganite vs quartz diagram (Fig. 4G), showing a moganite content in the range 3–20 wt%. The samples seem to be divided into two major groups separated by a small gap at moganite content around 7 wt%. It should be investigated on a larger number of samples whether this is a true indication of different geological sources, or rather a bias due to the limited number of samples; however, it is worth underlining that cherts and carnelians do not group under separate compositions.

A few samples show a slightly larger amount of moganite (samples 6B, 2D, and 22), although this mineralogical feature seems to be uncorrelated to any chemical variable, so that no geological or genetic or weathering significance can be proposed at this stage. Finally, the carnelian sample 3 (from Saniat Jibril) is distinguished from the entire collection based on nearly equal contents of quartz and moganite. It has been proposed that moganite crystallisation should be related to highly alkaline fluids coupled with high iron activity (Heaney, 1995).

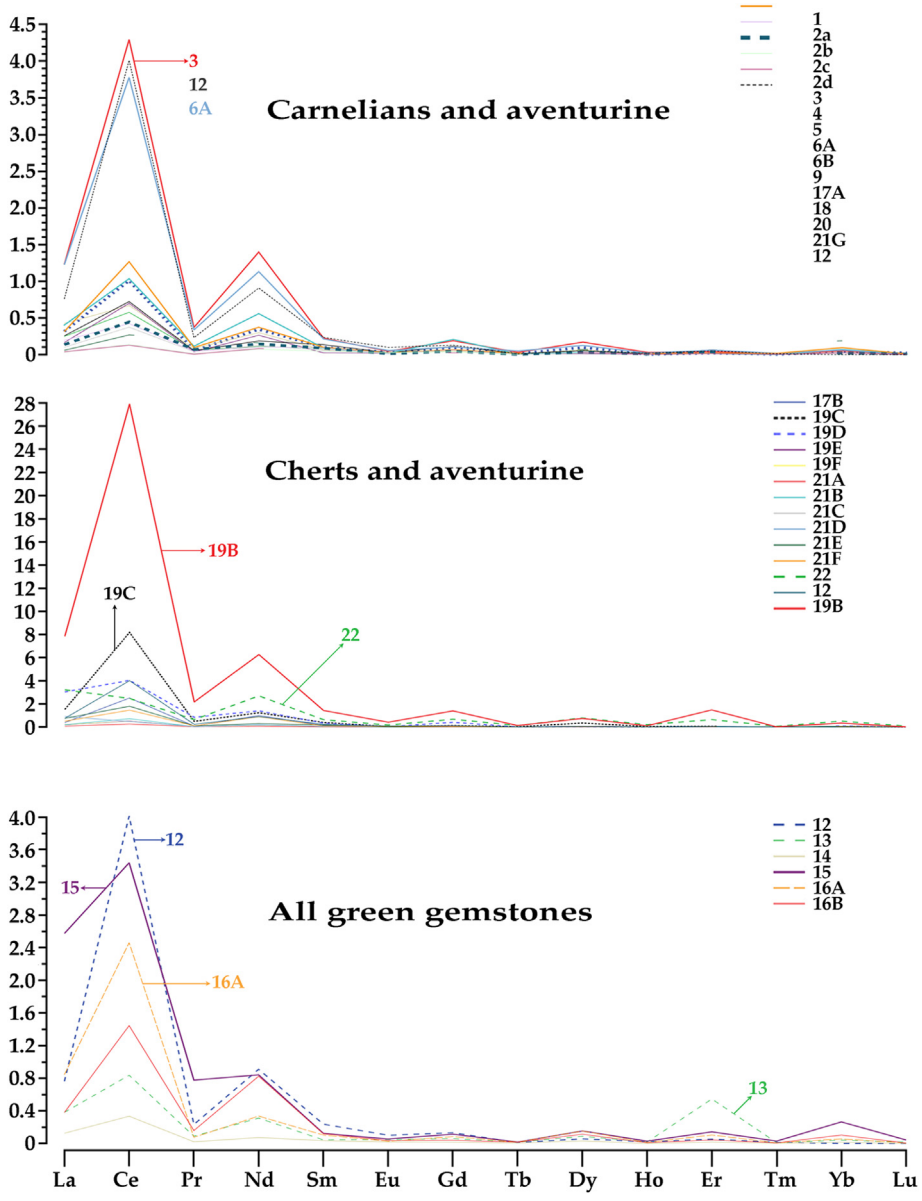

Fig. 5. LA-ICP-MS results: the REE pattern. All values are expressed in ppm.

In this regard, sample 3 shows slightly higher CaO and FeO contents than the average values obtained for both carnelians and cherts, and the highest MgO contents of both groups. The quartz:moganite ratio, the chemical composition in terms of minor element content and the REE pattern should be clearly related to a different geological occurrence of the carnelian no. 3 with respect to the other analysed samples.

Fig. 6 shows the correlation between the values of the quartz/moganite ratio obtained by Raman spectroscopy and those obtained by Rietveld analysis. Taking into account the instrumental difficulties and theoretical biases intrinsic in both techniques, the inter-calibration results are extremely satisfactory and they clearly indicate that when experiments and data analysis are carefully performed both techniques yield reasonable assessment of the mineral phase quantities.

4.2. The database for silica based materials: a new tool for provenance

The preliminary characterisation of the Libyan carnelians and cherts indicates specific signatures in terms of trace elemental composition and quartz/moganite ratio. Given that one of the objectives of this study is to provide a frame for provenance discrimination, a database was organised encompassing the chemical data (minor and trace elements) available in the literature for similar materials. Although largely available and undoubtedly necessary to identify the petrology and mineralogy of the rock, the major elements were discarded because they proved to be inappropriate in terms of provenance discrimination.

The sample totals in the database (see the "Appendix: the database" for all details) are as follows: 1180 entries representing more than 1520 samples, classified according to authors into chert (512), quartzite (402), flint (191), agate (138), opal (134), chalcedony (>71), quartz (31), carnelian (17), jasper (12), hornstone (5), quartz-chert (5), amethyst (1), and chrysoprase (1 or more) from 37 nations. The uncertainty on the total samples number is due to the fact that some authors used generic indications as "many samples" or just the plural "samples" without specifying the exact number.

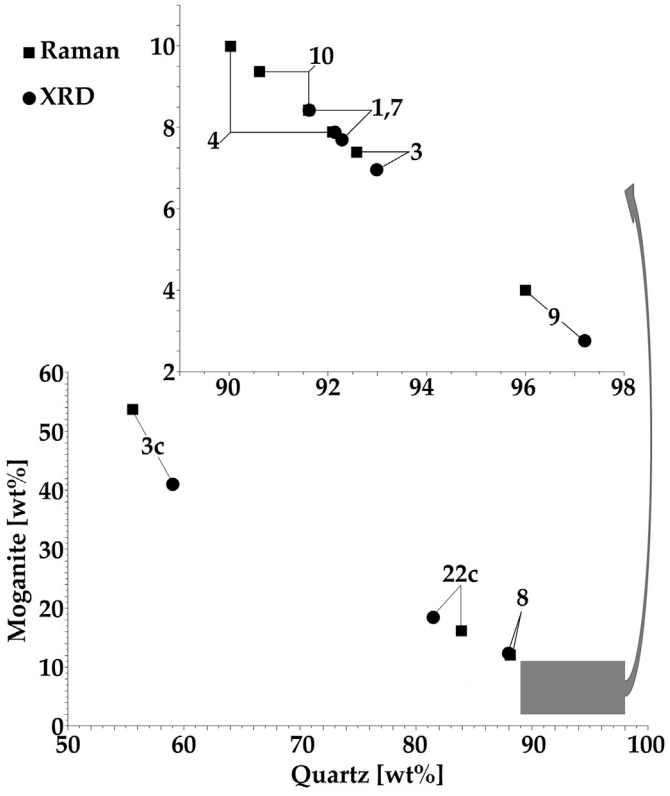

Fig. 6. The quartz/moganite ratio established by Raman spectroscopy and Rietveld analysis.

The analytical techniques used by the authors for trace element determination were ICP-MS, ICP-OES or ICP-AES, LA-ICP-MS and INAA. A total of four studies also used XRF, FAAS, PGA and spectral analyses for the investigation of 29 flints (Kasztovszkyet al., 2008 using PGAA), and 19 cherts (5 from Di Leo et al., 2002 using XRF; 5 from Misik, 1996 using spectral analyses and 9 from Migaszewski et al., 2006 using FAAS). The fact that a few analytical techniques were used for trace elements determination, made the data comparison possible, and the data set consistent. On the contrary, the plethora of techniques used for the determination of the major elements contents (SEM, EMPA, XRF and portable XRF, IBA, ICP-AES, ICP-MS, INAA, prompt gamma activation analysis, gravimetry, etc.) provided an additional reason not to use them for comparative purposes.

A further important consideration concerns the elements determined by the authors and, consequently, the possibility to deal with reference data. The descriptive statistics shown in Table 5 clearly demonstrate that the comparison of our data with available reference data is reliable only for some elements. This is to say that multivariate statistics becomes inappropriate; furthermore, a comparison based, for instance, on a single element (e.g. Be) may produce non representative results.

The comparison with the database is further complicated by the fact that some authors provide the results of the single measurements performed on the samples while others show the average values only. For this reason, the comparison has been based on the latter values, i.e. those that can be extracted or calculated from all references as well as for the present data.

The binary diagrams reported in Figs. 7–10 provide visual examples of the compositional distribution of the data. The Libyan materials analysed in the present work (carnelians and cherts) were grouped into a single mean chemical composition, except samples 3, 6a, 19b, and 21a, which were kept separate because of chemical differences.

The Libyan materials show a few general features: 1) cherts and carnelians generally plot next to each other in the concentration-poor area of the diagram; and 2) the bulk of Libyan samples are similar to the few published results from Indian, although they can be distinguished on the basis of the systematically larger contents of Ni, Cr, Zr, Ta, Sc, and Th–U ratio.

The large differences observed for the Libyan sample 19B with respect to the other Libyan samples is not easily explainable. The SEM images and elemental maps tend to rule out surface contamination or alteration processes. Similar considerations must be made for the samples 3, 6A and 21a, whose differences, however, are more limited to certain elements, such as the contents of Sc (Fig. 7) or the Ba– Sr (Fig. 8), La– Ce (Fig. 9) or Tb–Dy (Fig. 10) ratios.

In relation to the provenance problems, the comparison with the collected database allowed us to draw some general considerations. First, the different chemical composition seems adequate to exclude an Indian origin of the Libyan materials, as already suggested in the archaeological literature (Mattingly, 2013). This is supported by the fact that both the cherts and carnelians are compositionally very similar and it is inherently unlikely that the material was imported from India in its unreduced state to account for this. The geochemistry and the archaeological association between carnelian and chert debitage thus support a Saharan origin.

Secondly, the systematic depletion of a number of minor and trace elements in the Libyan materials allows us to consider these materials as representative of a single main source, with the possible exception of samples 3, 6a, 19a, and 21b. The evidence of primary processing of material from a single source may indicate that a Saharan source existed relatively close at hand to the Garamantian heartlands, with the balance of probability (based on the 19th-century travellers' accounts and the geology, favouring the Tibesti mountains to east of Tijirhi and al-Qatrun.

For the moment, the exact quarry site remains unknown. Future fieldwork might concentrate on the west side of Tibesti and the route running north from there to Fazzan. We might note that 19a and 21b are from large debitage deposits that on other grounds we would have expected to represent homogenous

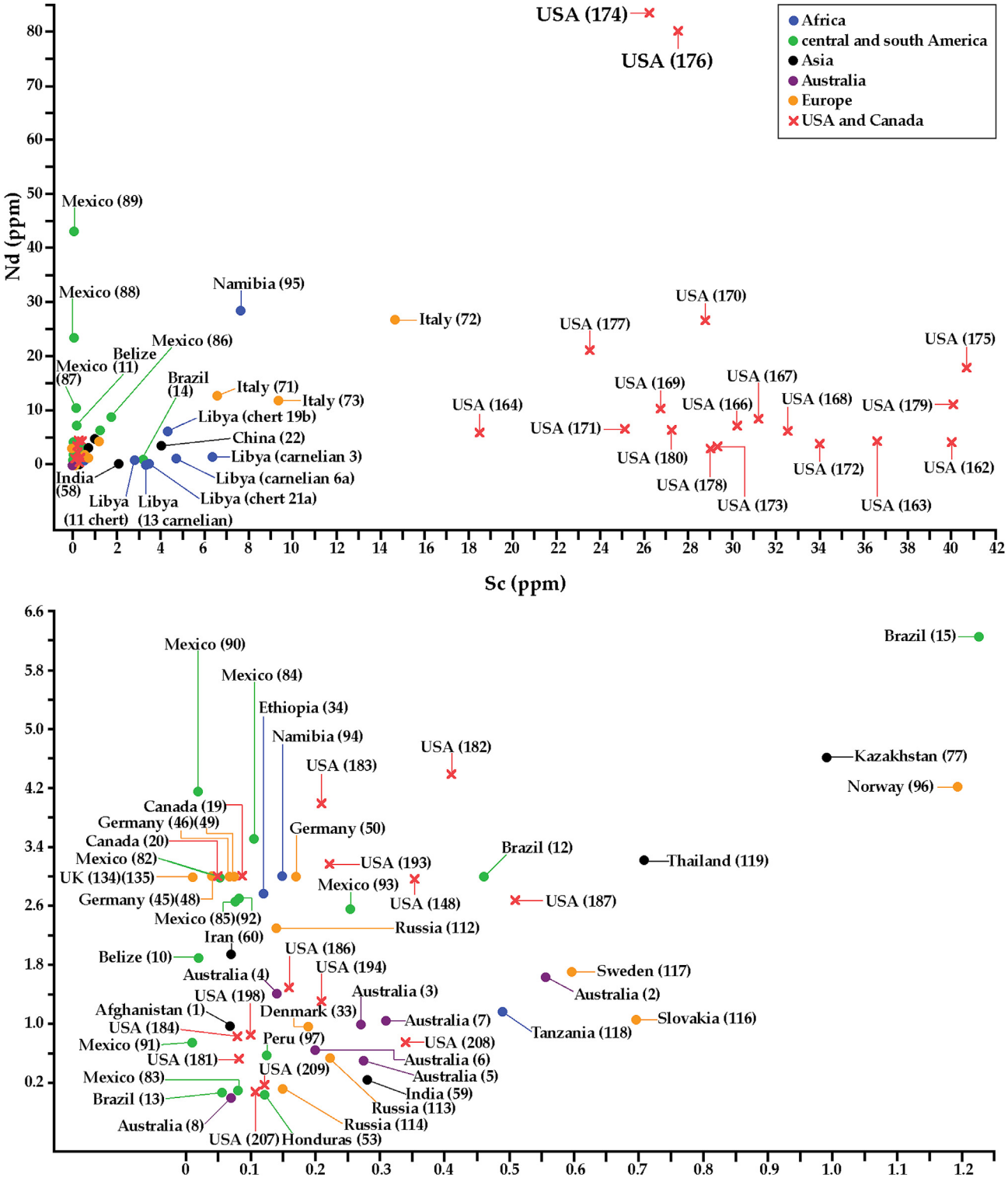

Fig. 7. LA-ICP-MS results: Sc – Nd binary diagram. In order to show the distribution of all available data, the lower diagram shows the magnification of a small portion of the upper one. The axis titles are the same in all plots. The numbers are those listed as in the Appendix.

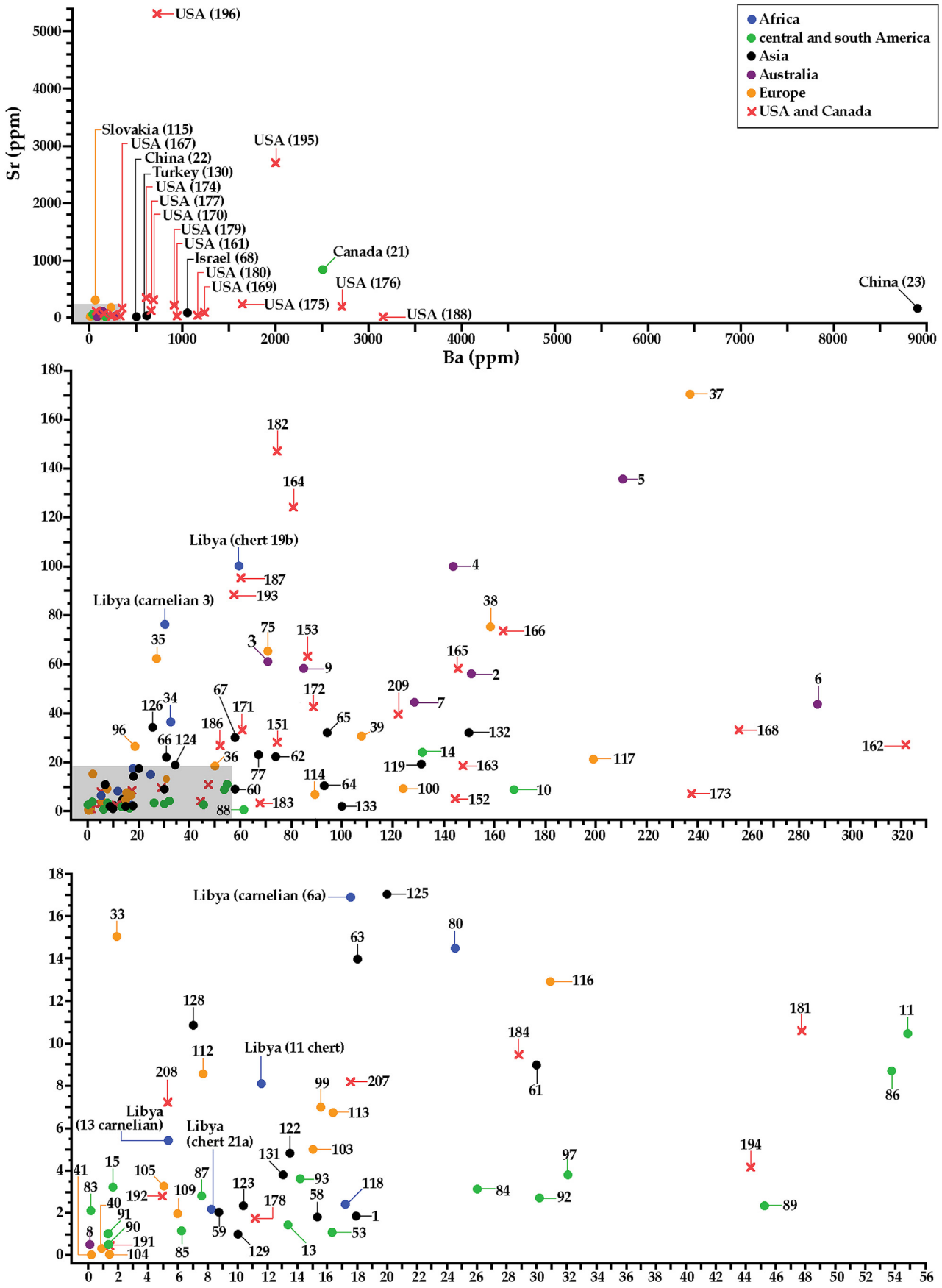

Fig. 8. LA-ICP-MS results: Ba– Sr binary diagram. In order to show the distribution of all available data, the lower diagrams show progressive magnifications of a small portion of the upper ones. The axis titles are the same in all plots. The numbers are those listed as in the Appendix.

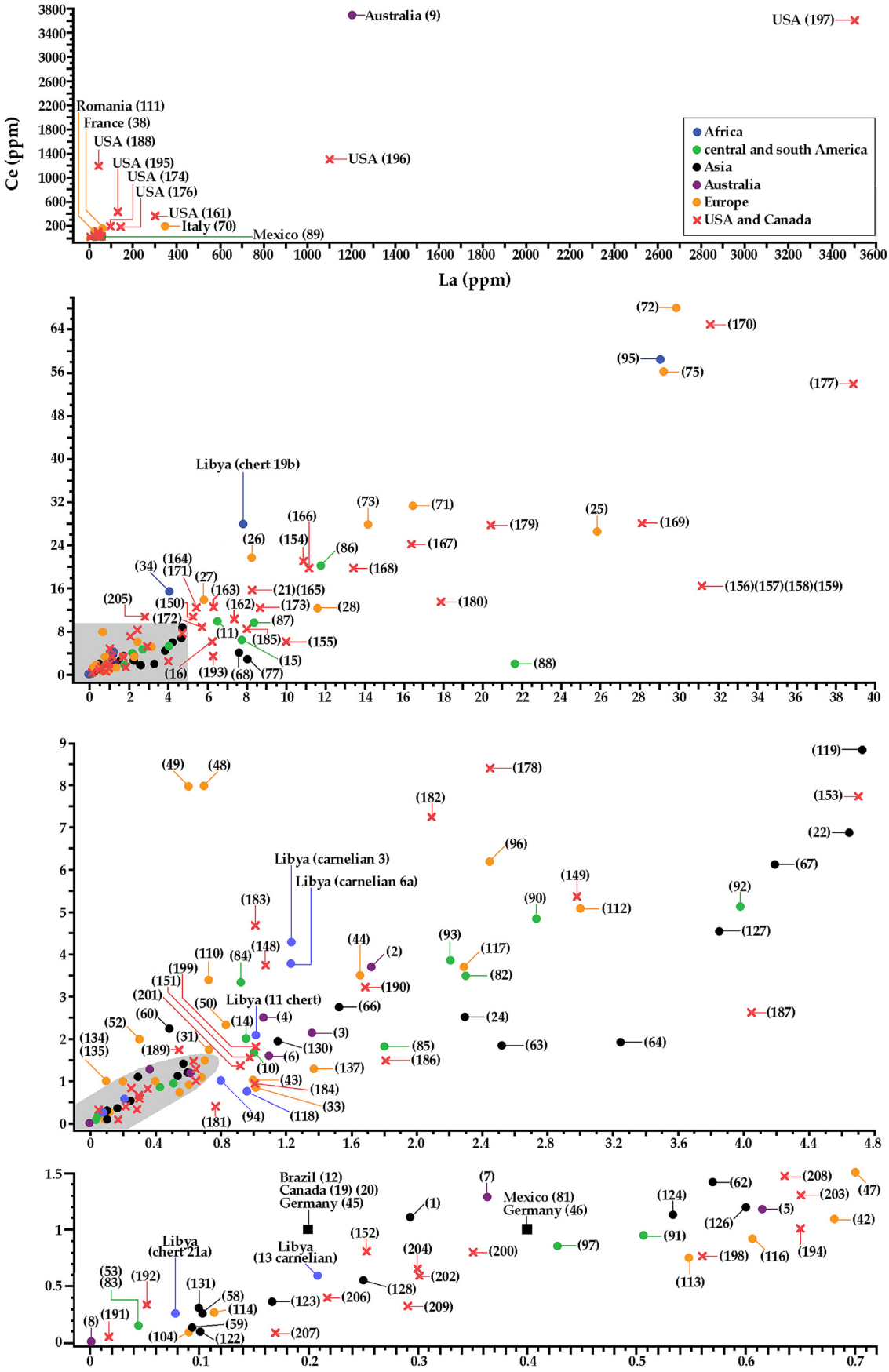

Fig. 9. LA-ICP-MS results: La– Ce binary diagram. In order to show the distribution of all available data, the lower diagrams show progressive magnifications of a small portion of the upper ones. The axis titles are the same in all plots. The numbers are those listed as in the Appendix.

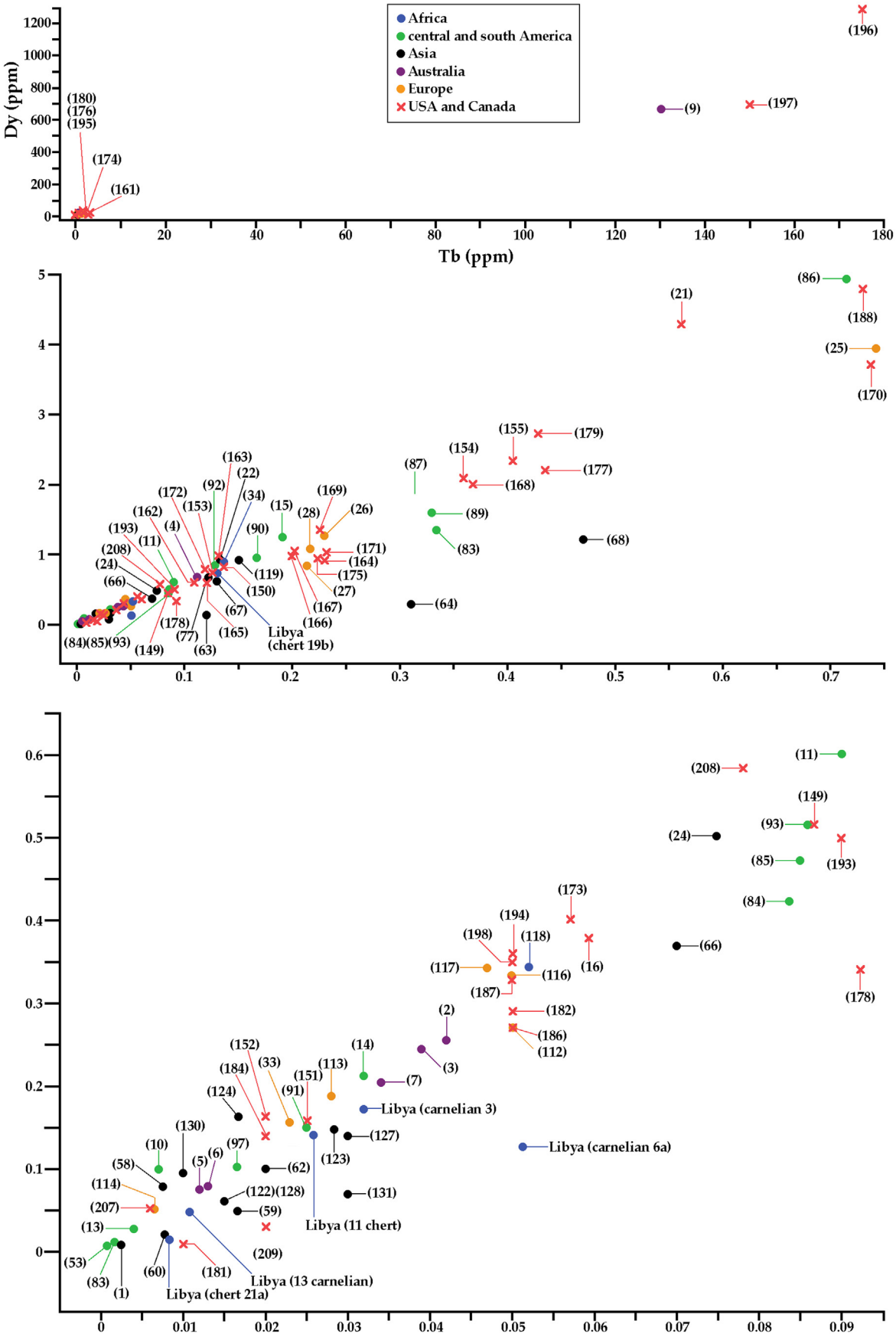

Fig. 10. LA-ICP-MS results: Tb–Dy binary diagram. In order to show the distribution of all available data, the lower diagrams show progressive magnifications of a small portion of the upper ones. The axis titles are the same in all plots. The numbers are those listed as in the Appendix.

processing debris. Overall, the relative homogeneity of the material from Garamantian sites suggests that most was obtained from a single source, though the trace element outliers probably indicate some trade or transport of material from elsewhere in the Sahara.

Thirdly, leaving momentarily aside the Indian materials, it is worth noting that the chemical composition of the samples in the database allows us to bring several reference groups close to the Libyan materials, however, these always change depending on which elements are considered. This evidence reinforces even more the possibility that we can discriminate between the Libyan materials and agate, flint, chalcedony, etc., from other parts of the world.

Finally, the lack of comparative data must be underlined, in relation to both material type (carnelian analysis remains rare in literature) and geographic origin (more material of West African and Saharan origin needs analysing). In the Mediterranean world, carnelian was commonly employed as engraved bezels for sealing rings (intaglio rings). The new information on the compositional signature of Saharan carnelian now offers the possibility of testing assemblages of carnelian intaglios from within the Roman empire to determine whether the material came from an Indian or a Saharan source.

4.3. Green samples: amazonites

Based on chemical and mineralogical characterisation, the green samples can be shown to be of two different lithotypes. Sample 12 is constituted of quartz including tiny crystals of a Cr-rich phyllosilicate. Although the SEM data did not allow us to distinguish fuchsite from Cr-illite (Table 6), it is nonetheless possible to assign it the generic name of “aventurine”. All the other samples are essentially composed of K-feldspar, with minor plagioclase, quartz and muscovite. Hence, the initial assignment to amazonite is definitely confirmed. The origin of amazonite circulating in Northern Africa is debated, since it was widely used in ancient Egypt, although there is no known source close to the Nile Valley. It is often assumed in the literature that amazonite was traded to Egypt from the Tibesti occurrence at Eghei Zuma (De Michele and Piacenza, 1999), although equally rich sources are present in Ethiopia and elsewhere. Tentative discrimination of sources has recently been attempted based on minor elements analysis by EPMA (Zerboni and Vignola, 2013). The peculiar and consistent REE pattern measured in the present study for the Libyan archaeological samples (Table 7, Fig. 5) could indicate further discriminating parameters for provenancing the amazonite occurrences.

Acknowledgements

The analyses reported on here were carried out as part of the work of the Trans-SAHARA project, supported by the European Research Council under the European Union's Seventh Framework Programme (FP/2007-2013)/ERC Grant Agreement no. 269418. All analyses were carried out by EG and GA, using samples provided by the Trans-SAHARA team, with all authors contributing to the writing up of the results. Professor Michael D. Glascock is gratefully acknowledge for sharing his data on Indian carnelians. F. Zorzi kindly helped in the XRPD data collection.

Appendix. The database

Data mining was performed by searching the web scientific libraries through several keywords: “agate”, “carnelian”, “chalcedony”, “chert”, ”flint”, “hornstone”, “moganite”, “opal”, and “quartz”, combined with “trace element” and/or “geochemistry”. The search accepted only the papers including the selected keywords as the main topic. Materials from Japan as well as oceanic materials were excluded for geographical reasons; conversely data referring to Northern and Southern America and China were accepted because they are actual sources of precious stones, and archaeometric discrimination could well serve for identification of fakes.

Despite the large number of references initially found (>1100), it was soon clear that most papers did not report chemical data. Most of them dealt with TL and/or OSL dating of burnt flint (e.g. Guérin et al., 2012; Schmidt et al., 2013a; Mercier, et al., 2013); use-wear by laser profilometry (e.g. Stemp et al., 2009); heat treatments (e.g. Schmidt et al., 2012b; 2013b); engraving techniques (e.g. Sax et al., 1995, 1998; Rosenfeld et al., 2003); mechanical properties by geotechnical tests (e.g. Yonekura 2008; Tsobgou 2009); crystal properties and moganite content by X-ray diffraction (e.g. Pretola 2011; Gliozzo et al., 2011; Graetsch and Grünberg 2012); and petrological issues (e.g. Bustillo et al., 2009; Machado et al., 2013).

Valuable trace element concentrations were provided in a total of 20 archaeometric papers (Aspinall and Feather 1972; De Bruin et al., 1972; Luedtke 1978; Craddock et al., 1983; Hess 1996; Cackler et al., 1999; Nathan et al., 1999; Lyons et al., 2003; Glascock 2004; Insoll et al., 2004; Evans and Donahue 2005; Evans et al., 2007; Kasztovszky et al., 2008; Navazo et al., 2008; Huckell et al., 2011; Olofsson and Rodushkin 2011; Law et al., 2012; Pettitt et al., 2012; Pitblado et al., 2013; ten Bruggencate et al., 2013). After exclusion of those papers omitting data or including data that are incompatible because of instrumental protocols, it was possible to define a set of 12 papers reporting more than 1041 silica samples, including agate (80), chalcedony (11), chert (319), flint (189), opal (25) and quartzite (402). Provenance localities are as follows: Afghanistan (15), Belize (22), Czech Republic (1), Denmark (7), Hungary (9), India (30), Iran (15), Israel (102), Poland (6), Russia (12), Sweden (6), Thailand (20), The Netherlands (17), United Kingdom (>27), Ukraine (2), and USA (722).

The second group of papers derived from the geological literature: a total of 28 papers (Manetti et al., 1979; Murray et al., 1991, 1992; Becq-Giraudon et al., 1992; Misik 1996; Peng et al., 2000; Götze et al., 2001; Halamić et al., 2001; Di Leo et al., 2002; Marcoux et al., 2004; Grenne and Slack 2005; Amelin and Back 2006; Migaszewski et al., 2006; Gaillou et al., 2008; Chang et al., 2009; Götze et al., 2009; Möckel et al., 2009; Hatipoğlu et al., 2010; Simoni et al., 2010; Baldwin et al., 2011; Hatipoğlu et al., 2011a and 2011b; Karacik et al., 2011; Parali et al., 2011; Eker et al., 2012; Schmidt et al., 2012a; Caucia et al., 2012; Wang et al., 2012) including the measurements of >479 samples: agate (>58), amethyst (1), carnelian (2), chalcedony (>59), chert (193), chrysoprase (1 or >1), flint (2), hornstone (5), jasper (12), opal (109), quartz (31) and quartz-chert (5), from Australia (12), Brazil (7), Canada (10), China (59), Croatia (42), Czech Republic (6), Ethiopia (8), France (62), Germany (30), Honduras (7), Italy (21), Kazakhstan (3), Madagascar (4), Mexico (35), Namibia (3), Norway (12), Peru (2), Poland (19), Romania (4), Slovakia (4), Tanzania (2), Turkey (30), UK (4), and USA (93).

As far as the composition, those papers reporting measurements on siliceous rocks with SiO_2 <70 wt% were excluded. Moreover, a difference between “entries” and “samples” was taken into account, given that some authors provided the mean values for a collection of samples or provided multiple measurements for the same sample.

Summary of data extracted from references, ordered based on nation.

"#"	Progressive number reported in Figures 7–10
"A/G"	Archaeological or geological
"Entries"	Given that measurements are provided for a single specimen or as the average value of a sampleset, the number of entries sometimes differed from that of samples
"Samples"	The number of samples investigated by the Authors
"Materials"	Abbreviations: QTZ = quartz; QTE = quartzite; ATH = Amethyst; CED = Chalcedony; CAR = Carnelian; CHR = Chrysoprase; OPA = Opal (followed by the indication of the different varieties A or C or CT if specified); POR = porcellanite; DIA = diatomite; AGA = agate; CRT = Chert, FLT = Flint, HOR = Hornstone, JAS = Jasper.
"Locality"	Brief geographic indications. Abbreviations: F. = Formation; UGB = UGB; WRGS = WRGS.
"Age"	As provided by Authors.
"Analytical technique"	NAA = Neutron activation analysis; PGAA = prompt gamma activation analysis; LA-ICP-MS = Laser ablation inductively coupled plasma mass spectrometry; ICP-MS = inductively coupled plasma mass spectrometry; ICP–SFMS = inductively coupled plasma – sector field mass spectrometry; MC–ICP–MS = Multicollector-Inductively Coupled Plasma Mass Spectrometry; ICP-AES = inductively coupled plasma atomic emission spectrometry; XRF = X-ray fluorescence; FAAS = flame atomic absorption spectrometry; AA = Atomic Absorption; ES = emission spectrometry; G = gravimetry; CT=coulometric tritation; C = combustion.
"Reference"	Abbreviation: p.c. = personal communication.

#	A/G	Country	Entries	Samples	Locality	Analytical technique	Dating	Reference
1	A	Afghanistan	15	15 AGA	–	NAA	–	Law et al., 2012
2	G	Australia	12	3 OPA	NSW, Lightning Ridge	ICP-MS	–	Gaillou et al., 2008
3	G			2 OPA	NSW,Tintenbar	ICP-MS	–	Gaillou et al., 2008
4	G			1 OPA	SA, Andamooka	ICP-MS	–	Gaillou et al., 2008
5	G			2 OPA	SA, Coober Pedy	ICP-MS	–	Gaillou et al., 2008
6	G			1 OPA	SA, Mintabie	ICP-MS	–	Gaillou et al., 2008
7	G			1 OPA	SA, Quilpie	ICP-MS	–	Gaillou et al., 2008
8	G			1 OPA	WA, Norseman	ICP-MS	–	Gaillou et al., 2008
9	G			1 OPA	–	ICP-MS	–	Amelin and Back 2006
10	A	Belize	2	11 CED	Crooked tree	NAA	–	Cackler et al., 1999
11	A			11 CRT	Crooked tree	NAA	–	Cackler et al., 1999
12	G	Brazil	7	1 AGA	Rio Grande do Sul	NAA[a]	Cretaceous	Götze et al., 2001 [c]
13	G			2 OPA	Para	ICP-MS	–	Gaillou et al., 2008
14	G			2 OPA	Piaui, Pedro II	ICP-MS	–	Gaillou et al., 2008
15	G			2 OPA	Rio Grande do Sul	ICP-MS	–	Gaillou et al., 2008
16	G	Canada	35	3 CRT	Abitibi greenstone belt	LA-ICP-MS	Neoarchean	Baldwin et al., 2011
17	G			1 QTZ	Agate Island	NAA [a]	Precambrian	Götze et al., 2001 [d]
18				2 AGA	Agate Island	NAA [a]	Precambrian	Götze et al., 2001 [d]
19	G			2 AGA	Agate Point	NAA [a]	Precambrian	Götze et al., 2001 [d]
20	G			1 QTZ	Agate Point	NAA [a]	Precambrian	Götze et al., 2001 [d]
21	G			1 OPA-A	Kamloops Lake, British Columbia	ICP-MS	–	Amelin and Back 2006
22	G	China	59	17 CRT	Liuchapo F. in the Liuchapo section of central Hunan Province	XRF;ICP-MS	Ediacaran–Cambrian	Chang et al., 2009
23	G			17 CRT	Yangtze plate	NAA	Upper Sinian	Peng et al., 2000
24	G			25 CRT	Yangtze Platform, western Hunan -	XRF;ICP-MS	Ediacaran–Cambrian	Wang et al., 2012
25	G	Croatia	42	7 CRT	Ivanščica	XRF; ICP-MS	Triassic	Halamić et al., 2001
26	G			14 CRT	Kalnik	XRF; ICP-MS	Triassic	Halamić et al., 2001
27	G			11 CRT	Medvednica	XRF; ICP-MS	Triassic	Halamić et al., 2001
28	G			10 CRT	Žumberak	XRF; ICP-MS	Triassic	Halamić et al., 2001
29	G	Czech Republic		2 AGA	Frýdštejn, Bohemia	NAA[a]	Permocarboniferous	Götze et al., 2001 [e]
30	G			2 AGA	Frýdštejn, Bohemia	NAA[a]	Permocarboniferous	Götze et al., 2001 [e]
31	G			4 AGA	Nova Paka, Bohemia	NAA[a]	Permocarboniferous	Götze et al., 2001 [e]
32	A			1 FLT	Marsovice	PGAA	–	Kasztovszky et al., 2008
33	A	Denmark	7	7 FLT	–	ICP–SFMS; MC–ICP–MS	–	Olofsson and Rodushkin 2011
34	G	Ethiopia	8	8 OPA	–	ICP-MS	–	Gaillou et al., 2008
35	G	France	62	1 CRT	Col des Castans, Assignan, Herault	XRF, ICP	Ordovician	Becq-Giraudon et al., 1992
36	G			1 CRT	La Maurerie, Herault	XRF, ICP	Ordovician	Becq-Giraudon et al., 1992
37	G			1 CRT	Le Puech de Lugne, Lugne, Herault	XRF, ICP	Ordovician	Becq-Giraudon et al., 1992
39	G			2 CRT	Traveusot, Guichen (Ille-et-Vilaine)	XRF, ICP	Ordovician	Becq-Giraudon et al., 1992
38	G			57 CED	Northern Massif Central	XRF;ICP-MS	Permian	Marcoux et al., 2004
40	G	Germany	22	5 AGA	Chemnitz	LA-ICP-MS	–	Götze et al., 2009 [j]
41	G			5 QTZ	Chemnitz	LA-ICP-MS	–	Götze et al., 2009 [j]
42	G			5 HOR	Dinkelberg, Baden-Württemberg	LA-ICP-MS	Middle Triassic	Schmidt et al., 2012a
43	G			1 QTZ	Gröppendorf	NAA[a]	Permocarboniferous	Götze et al., 2001 [h]
44	G			2 AGA	Gröppendorf	NAA[a]	Permocarboniferous	Götze et al., 2001 [h]
45	G			1 QTZ	Halsbach	NAA[a]	Permocarboniferous	Götze et al., 2001 [h]
46	G			2 AGA	Halsbach	NAA[a]	Permocarboniferous	Götze et al., 2001 [h]
47	G			2 AGA	Idar–Oberstein	NAA[a]	Permocarboniferous	Götze et al., 2001 [f]
48	G			1 ATH	Lauterbach	NAA[a]	Permocarboniferous	Götze et al., 2001 [g]

(*continued*)

#	A/G	Country	Entries	Samples	Locality	Analytical technique	Dating	Reference
49	G			1 QTZ	Lauterbach	NAA[a]	Permocarboniferous	Götze et al., 2001 [g]
50	G			3 AGA	Lauterbach	NAA[a]	Permocarboniferous	Götze et al., 2001 [g]
51	G			1 AGA	Schlottwitz	NAA[a]	Permocarboniferous	Götze et al., 2001 [i]
52	G			1 QTZ	Schlottwitz	NAA[a]	Permocarboniferous	Götze et al., 2001 [i]
53	G	Honduras	7	7 OPA	–	ICP-MS	–	Gaillou et al., 2008
54	A	Hungary	9	2 FLT	Bodrogkeresztúr	PGAA	–	Kasztovszky et al., 2008
55	A			3 FLT	Esztergom	PGAA	–	Kasztovszky et al., 2008
56	A			3 FLT	Nadap	PGAA	–	Kasztovszky et al., 2008
57	A			1 FLT	Nagytevel	PGAA	–	Kasztovszky et al., 2008
58	A	India	30	15 AGA	Mardet Bet, Gujarat	NAA	–	Law et al., 2012
59	A			15 AGA	Ratanpur, Gujarat	NAA	–	Law et al., 2012
60	A	Iran	15	15 AGA	Shahr-i-Sokhta	NAA	–	Law et al., 2012
61	A	Israel	8	8 FLT	Bina F.[o]	ICP-MS/OES	Turonian	Nathan et al., 1999
62	A			19 FLT	Deir Hanna F.[o]	ICP-MS/OES	Cenomanian	Nathan et al., 1999
63	A			6 FLT	likely Deir Hanna F.[o]	ICP-MS/OES	–	Nathan et al., 1999
64	A			3 FLT	likely Zor'a F.[o]	ICP-MS/OES	–	Nathan et al., 1999
65	A			6 FLT	Mishash F.[o]	ICP-MS/OES	Campanian	Nathan et al., 1999
66	A			20 FLT	Yanuh F.[o]	ICP-MS/OES	Cenomanian- Turonian	Nathan et al., 1999
67	A			20 FLT	Yirka F.[o]	ICP-MS/OES	Turonian	Nathan et al., 1999
68	A			20 FLT	Zor'a F.[o]	ICP-MS/OES	Eocene	Nathan et al., 1999
69	G	Italy	21	2 OPA	Baldissero Canavese, Turin	LA-ICP-MS	–	Caucia et al., 2012
70	G			2 FLT	Caredo, Lessinian Mountains	LA-ICP-MS	–	Schmidt et al., 2012a
71	G			3 CRT	Graveglia Valley, loc. Ponte di Lagoscuro	NAA	Jurassic	Manetti et al., 1979
72	G			2 CRT	Graveglia Valley, loc. S. Rocco	NAA	Jurassic	Manetti et al., 1979
73	G			4 CRT	Lima Valley	NAA	Jurassic	Manetti et al., 1979
74	G			2 OPA	Mt. Calvo at Caselette, Turin	LA-ICP-MS	–	Caucia et al., 2012
75	G			5 CRT	Scisti silicei F. (Potenza and Mt. Sellata)	XRF	Jurassic	Di Leo et al., 2002
76	G			1 OPA	Siulius, Cagliari	LA-ICP-MS	–	Caucia et al., 2012
77	G	Kazakhstan	3	3 OPA	–	ICP-MS	–	Gaillou et al., 2008
78	A	Libya	28	13 CRT	Lybia	LA-ICP-MS	–	present work
79	A			15 CAR	Lybia	LA-ICP-MS	–	present work
80	G	Madagascar	4	4 OPA	Bemia	LA-ICP-MS	Cretaceous	Simoni et al., 2010
81	G	Mexico	35	1 QTZ	Chihuahua	NAA[a]	Tertiary	Götze et al., 2001 [k]
82	G			2 AGA	Chihuahua	NAA[a]	Tertiary	Götze et al., 2001 [k]
83	G			3 OPA	Durango, Mapimi	ICP-MS	–	Gaillou et al., 2008
84	G			6 OPA	Jalisco, Los Laureles	ICP-MS	–	Gaillou et al., 2008
85	G			2 OPA	Jalisco, Lupita	ICP-MS	–	Gaillou et al., 2008
86	G			3 OPA	Jalisco, San Martin	ICP-MS	–	Gaillou et al., 2008
87	G			5 OPA	Nayarit, Guadalupa	ICP-MS	–	Gaillou et al., 2008
88	G			1 OPA	Queretaro, Carbonera	ICP-MS	–	Gaillou et al., 2008
89	G			4 OPA	Queretaro, Cerro Viejo	ICP-MS	–	Gaillou et al., 2008
90	G			2 OPA	Queretaro, Guacamaya	ICP-MS	–	Gaillou et al., 2008
91	G			2 OPA	Queretaro, Iris	ICP-MS	–	Gaillou et al., 2008
92	G			2 OPA	Queretaro, La Fe	ICP-MS	–	Gaillou et al., 2008
93	G			2 OPA	Queretaro, Olimpia	ICP-MS	–	Gaillou et al., 2008
94	G	Namibia	3	1 AGA	Sarusa mine	NAA[a]	Cretaceous	Götze et al., 2001 [l]
95	G			2 QTZ	Sarusa mine	NAA[a]	Cretaceous	Götze et al., 2001 [l]
96	G	Norway	12	12 JAS	Løkken ophiolite	XRF;NAA; ICP-AES;AA; ES;G;CT; C[p]	Ordovician	Grenne and Slack 2005
97	G	Peru	2	2 OPA	Acari	ICP-MS	–	Gaillou et al., 2008
98	A	Poland	17	1 FLT	Beblo	PGAA		Kasztovszky et al., 2008
99	G			2 CRT	Głuchowiec; Holy Cross Mountains	ICP-AES; FAAS[b]	Oxfordian- Kimmeridgian	Migaszewski et al., 2006
100	G			2 CRT	Iłża; Holy Cross Mountains	ICP-AES; FAAS[b]	Oxfordian- Kimmeridgian	Migaszewski et al., 2006
101	A			1 FLT	Krzemionki	PGAA	–	Kasztovszky et al., 2008
102	A			1 FLT	Maków	PGAA	-	Kasztovszky et al., 2008
103	G			4 CRT	Morawica; Holy Cross Mountains	ICP-AES; FAAS[b]	Oxfordian- Kimmeridgian	Migaszewski et al., 2006
104	G			5 AGA	Nowy Kościoł	LA-ICP-MS	Permian	Möckel et al., 2009
105	G			5 QTZ	Nowy Kościoł	LA-ICP-MS	Permian	Möckel et al., 2009
106	A			1 FLT	Poland – Saspów	PGAA	–	Kasztovszky et al., 2008
107	A			1 FLT	Swieciechów	PGAA	-	Kasztovszky et al., 2008
108	A			1 FLT	Wierzbycza	PGAA	–	Kasztovszky et al., 2008
109	G			1 CRT	Wojciechówka; Holy Cross Mountains	ICP-AES; FAAS[b]	Oxfordian- Kimmeridgian	Migaszewski et al., 2006
110	G	Romania	4	2 CAR	Coşava, Banat	LA-ICP-MS	–	Schmidt et al., 2012a
111	G			2 CED	Românești, Banat	LA-ICP-MS	–	Schmidt et al., 2012a

(*continued on next page*)

(*continued*)

#	A/G	Country	Entries	Samples	Locality	Analytical technique	Dating	Reference
112	A	Russia	12	1 FLT	Moscow area	ICP–SFMS; MC–ICP–MS	-	Olofsson and Rodushkin 2011
113	A			5 FLT	Valdai area	ICP–SFMS; MC–ICP–MS	–	Olofsson and Rodushkin 2011
114	A			6 FLT	White Sea area	ICP–SFMS; MC–ICP–MS	–	Olofsson and Rodushkin 2011
115	G	Slovakia	4	2 CRT	Carpathian Keuper, loc. Belanská Kotlina	Spectral an.	Triassic	Misik 1996
116	G			2 OPA	-	ICP-MS	–	Gaillou et al., 2008
117	A	Sweden	6	6 FLT	Vuollerim	ICP–SFMS; MC–ICP–MS	–	Olofsson and Rodushkin 2011
118	G	Tanzania	2	2 OPA	Tanzania	ICP-MS	–	Gaillou et al., 2008
119	A	Thailand	20	20 AGA	Thailand – Ban Khao Mogun	NAA	–	Law et al., 2012
120	A	The Netherlands	35	15 FLT	Rijckholt	NAA	–	De Bruin et al., 1972
121	A			2 FLT	–		–	De Bruin et al., 1972
122	G	Turkey	30	1 CRT	–	ICP-MS	Lias	Eker et al., 2012
123	G			6 CRT	Akcakale	ICP-MS	Lias	Eker et al., 2012
124	G			6 CRT	Alemdar	ICP-MS	Lias	Eker et al., 2012
125	G			2 CHR	Biga–Çanakkale	XRF;ICP-AES	–	Hatipoğlu et al., 2011b
126	G			1 AGA	Dereyalakvillage, Eskisehir	ICP-AES	Pliocene	Parali et al., 2011
127	G			2 OPA	Gümüldür region of western Anatolia	ICP-MS	11.3–12.5 Ma	Karacik et al., 2011
128	G			6 CRT	Pirahmet	ICP-MS	Lias	Eker et al., 2012
129	G			"many"CED	Saricakaya-Eskişehir	XRF;ICP-AES	–	Hatipoğlu et al., 2010
130	G			2 CRT	Tedas	ICP-MS	Lias	Eker et al., 2012
131	G			3 CRT	Tekke	ICP-MS	Lias	Eker et al., 2012
132	G			1 or >1 AGA	Çubuk, Ankara	XRF;ICP-AES	Miocene Period[q]	Hatipoğlu et al., 2011a
133	G			1 or >1 AGA	Çubuk, Ankara	XRF;ICP-AES	Miocene Period[q]	Hatipoğlu et al., 2011a
134	G	UK	33	1 AGA	Ardownie Quarry, Scotland	NAA [a]	Devonian	Götze et al., 2001 [m]
135	G			1 QTZ	Ardownie Quarry, Scotland	NAA [a]	Devonian	Götze et al., 2001 [m]
136	A			>1 FLT	Blackpatch	NAA	–	Aspinall and Feather 1972
137	A			20 FLT	Cissbury	NAA	–	Aspinall and Feather 1972
138	A			>1 FLT	Easton Down	NAA	–	Aspinall and Feather 1972
139	A			>1 FLT	Grand Pressigny	NAA	–	Aspinall and Feather 1972
140	A			>1 FLT	Grimes Graves	NAA	–	Aspinall and Feather 1972
141	G			1 AGA	Montrose, Scotland	NAA [a]	Devonian	Götze et al., 2001 [m]
142	G			1 QTZ	Montrose, Scotland	NAA [a]	Devonian	Götze et al., 2001 [m]
143	A			>1 FLT	Peppard	NAA	–	Aspinall and Feather 1972
144	A			>1 FLT	Spiennes	NAA	–	Aspinall and Feather 1972
145	A			>1 FLT	St. Gertrude and Rijkholt	NAA	–	Aspinall and Feather 1972
146	A	Ukraine[n]		1 FLT	Volhynia	PGAA	–	Kasztovszky et al., 2008
147	A			1 FLT	Prut	PGAA	–	Kasztovszky et al., 2008
148	A	USA	562	3 CRT	Beach Clovis cache site	NAA	Eocene-Oligocene	Huckell et al., 2011
149	G			3 CRT	California – Claremont F. (Monterey F.)	XRF, ICP-MS	Miocene	Murray et al., 1991
150	G			8 OPA	California – Elwood Beach (Monterey F.)	XRF, ICP-MS	Miocene	Murray et al., 1992
151	G			4 OPA	California – Jalama Canyon (Monterey F.)	XRF, ICP-MS	Miocene	Murray et al., 1992
152	G			5 QTZ	California – Jalama Canyon (Monterey F.)	XRF, ICP-MS	Miocene	Murray et al., 1992
153	G			2 OPA	California – Manville Diatomite Quarry (Monterey F.)	XRF, ICP-MS	Miocene	Murray et al., 1992
154	G			19 CRT	California – Marin Headlands, San Francisco (Ocean Basin)	XRF, ICP-MS	Mesozoic	Murray et al., 1991
155	G			9 CRT	California – Marin Headlands, San Francisco (spreading ridge)	XRF, ICP-MS	Mesozoic	Murray et al., 1991
156	G			5 CRT	California – Red Lassic Peak (Franciscan Complex)	XRF, ICP-MS	Mesozoic	Murray et al., 1991
157	G			5 CRT	California – Red Lassic Peak (Franciscan Complex)	XRF, ICP-MS	Mesozoic	Murray et al., 1991
158	G			5 CRT	California – Red Lassic Peak (Franciscan Complex)	XRF, ICP-MS	Mesozoic	Murray et al., 1991
159	G			5 CRT	California – Red Lassic Peak (Franciscan Complex)	XRF, ICP-MS	Mesozoic	Murray et al., 1991
160	G			5 CRT	California – Red Lassic Peak (Franciscan Complex)	XRF, ICP-MS	Mesozoic	Murray et al., 1991
161	A			3 QTE	Colorado – UGB -Black Canyon schist	LA-ICP-MS	Precambrian	Pitblado et al., 2013
162	A			10 QTE	Colorado – UGB – Cambrian Saguache	LA-ICP-MS	Cambrian	Pitblado et al., 2013
163	A			21 QTE	Colorado – UGB – Dakota/Burro Canyon	LA-ICP-MS	Cretaceous	Pitblado et al., 2013
164	A			6 QTE	Colorado – UGB – Dakota/Burro Canyon/Morrison	LA-ICP-MS	Cretaceous/Jurassic	Pitblado et al., 2013
165	A			10 QTE	Colorado – UGB – Debris flow gravels	LA-ICP-MS	Quaternary	Pitblado et al., 2013
166	A			10 QTE	Colorado – UGB – Fan gravels	LA-ICP-MS	Quaternary	Pitblado et al., 2013

(*continued*)

#	A/G	Country	Entries	Samples	Locality	Analytical technique	Dating	Reference
167	A			29 QTE	Colorado – UGB – Gravel deposit (Tertiary)	LA-ICP-MS	Tertiary	Pitblado et al., 2013
168	A			138 QTE	Colorado – UGB – Gravel deposit (unknown age)	LA-ICP-MS	Unknown	Pitblado et al., 2013
169	A			20 QTE	Colorado – UGB – Gravels (Quaternary)	LA-ICP-MS	Quaternary	Pitblado et al., 2013
170	A			10 QTE	Colorado – UGB – Gravels (Tertiary)	LA-ICP-MS	Tertiary	Pitblado et al., 2013
171	A			14 QTE	Colorado – UGB – Jurassic Entrada	LA-ICP-MS	Jurassic	Pitblado et al., 2013
172	A			59 QTE	Colorado – UGB – Jurassic Junction Creek	LA-ICP-MS	Jurassic	Pitblado et al., 2013
173	A			7 QTE	Colorado – UGB – Jurassic Morrison	LA-ICP-MS	Jurassic	Pitblado et al., 2013
174	A			9 QTE	Colorado – UGB – Quartzite dikes	LA-ICP-MS	Paleoproterozoic	Pitblado et al., 2013
175	A			10 QTE	Colorado – UGB – Quaternary fan gravels	LA-ICP-MS	Quaternary	Pitblado et al., 2013
176	A			10 QTE	Colorado – UGB – Quaternary gravels, alluvium	LA-ICP-MS	Quaternary	Pitblado et al., 2013
177	A			10 QTE	Colorado – UGB – River gravels, UGB	LA-ICP-MS	Modern	Pitblado et al., 2013
178	A			3 QTE	Colorado – UGB – Taylor River gravel	LA-ICP-MS	Contemporary	Pitblado et al., 2013
179	A			21 QTE	Colorado – UGB – Tertiary gravel and Tw deposit	LA-ICP-MS	Tertiary	Pitblado et al., 2013
180	A			2 QTE	Colorado – UGB	LA-ICP-MS	Paleoproterozoic	Pitblado et al., 2013
181	A			36 CRT	Colorado – WRGS – Flattop Butte	NAA	Eocene-Oligocene	Huckell et al., 2011
182	A			1 CRT	Dakota – WRGS – Sentinel Butte	NAA	Eocene-Oligocene	Huckell et al., 2011
183	A			49 CRT	Dakota – WRGS – Sentinel Butte	NAA	Eocene-Oligocene	Huckell et al., 2011
184	A			35 CRT	Dakota – WRGS – White River	NAA	Eocene-Oligocene	Huckell et al., 2011
185	A			17 CRT	Illinois – Cobden	NAA	–	Hess 1996 [r]
186	A			6 CRT	Indiana – Plummer, Spencer and Greene counties	NAA	–	Glascock 2004
187	A			10 CRT	Indiana – Wyandotte, Harrison county	NAA	–	Glascock 2004
188	G			2 OPA	Leo, Wyoming	ICP-MS	–	Amelin and Back 2006
189	A			10 CRT	Michigan – Bayport F., Huron and Arenac counties, Michigan	NAA	Upper Mississippian	Luedtke 1978
190	A			28 CRT	Michigan – Marshall F., Oceana County	NAA	Lower Mississippian	Luedtke 1978
191	G			10 QTZ	Montana – Bighorn district, Dryhead area	LA-ICP-MS	Permian	Götze et al., 2009
192	G			19 AGA	Montana – Bighorn district, Dryhead area	LA-ICP-MS	Permian	Götze et al., 2009
193	A			10 CRT	Nebraska – WRGS- Gering F.	NAA	Eocene-Oligocene	Huckell et al., 2011
194	A			28 CRT	Nebraska – WRGS- Knife River FLT	NAA	Eocene-Oligocene	Huckell et al., 2011
195	G			1 OPA	Nevada – Harper Valley	ICP-MS	–	Amelin and Back 2006
196	G			2 OPA	Nevada – Humboldt County, Nevada	ICP-MS	–	Amelin and Back 2006
197	G			1 OPA	Nevada – Virgin Valley	ICP-MS	–	Amelin and Back 2006
198	A			5 CRT	Ohio, FLT Ridge, Licking county	NAA	–	Glascock 2004
199	A			4 CRT	Oregon – Artifacts from the Mack Canyon Site	NAA	–	Hess 1996
200	A			2 CRT	Oregon – Gore Road Source near the Walaweeteese Quarry	NAA	Middle Miocene	Hess 1996
201	A			12 CRT	Oregon – Mack Canyon	ICP-MS	Lower to Middle Miocene	Hess 1996
202	A			2 CRT	Oregon – Railroad Tunnel Source west of the Deschutes River	NAA	Middle Miocene	Hess 1996
203	A			2 CRT	Oregon – Rock Creek – Goodnoe Hills	NAA	Middle Miocene	Hess 1996
204	A			2 CRT	Oregon – Spanish Hollow Source	NAA	Middle Miocene	Hess 1996
205	A			25 OPA	Oregon – Troy	NAA	-	Hess 1996 [s]
206	A			3 CRT	Oregon – Walaweeteese Quarry near Maryhill, Washington	ICP-MS	Middle Miocene	Hess 1996
207	G			2 OPA	Oregon – Opal butte	ICP-MS	–	Gaillou et al., 2008
208	G			1 OPA	Oregon – Owyhee	ICP-MS	–	Gaillou et al., 2008
209	A			30 CRT	Wyoming – WRGS – Table Mountain	NAA	Eocene-Oligocene	Huckell et al., 2011

[a] Except for Ti, Zr, Al, B, Ca, Mg, Mn and Cu, analysed by ICP-AES.
[b] FAAS for Al, As, Ba, Cd, Co, Cr, Cu, Fe, Mn, Mo, Ni, Pb, Sr, Ti, V, Zn, Zr; AAS for Hg.
[c] Reviewing data from Fallick et al. (1987).
[d] Reviewing data from McCrank et al. (1981).
[e] Reviewing data from Beer (1992).
[f] Reviewing data from Schmitt-Riegraf (1996).
[g] Reviewing data from Haake and Holzhey (1989).
[h] Reviewing data from Blankenburg (1988).
[i] Reviewing data from Haake et al. (1991).
[j] Reviewing data from Möckel and Götze (2007).
[k] Reviewing data from Cross (1996).
[l] Reviewing data from Harris (1989).
[m] Reviewing data from Fallick et al. (1985).
[n] Actually sampling was performed along the Prut and the Volhy Rivers in Romania and Moldavia, at the boundary with Ukraine.
[o] The numerous sampling sites are provided in the Appendix 1 of Nathan et al. (1999).
[p] Major elements by XRF; Au, Co, Cr, Rb, Cs, Hf, As, Sb, Sc, Ta, Th, U and REE by NAA; Ba, Y, Li, Mo, Nb, Sr, adn W by ICP-AES; Ag, Cu, Ge, Hg, Ni, Pb, Se, Te, V, and Zn atomic Absorption; B, Be, Bi, Cd, Sn, Ti, and Tl by emission spectrometry; FeO, H_2O, CO_2 and S by gravimetry, coulometric tritation and combustion.
[q] ~23.8–5.3y Mya.
[r] Data provided as personal communication to the Author from B. Ludtke
[s] Reviewing data from Cummings et al. 1989.

References

Amelin, Y., Back, M., 2006. Opal as a U-Pb geochronometer: search for a standard. Chem. Geol. 232, 67–86.

Aspinall, A., Feather, S.W., 1972. Neutron activation analysis of prehistoric flint mine products. Archaeometry 14, 41–53.

Baldwin, G.J., Thurston, P.C., Kamber, B.S., 2011. High-precision rare earth element, nickel, and chromium chemistry of chert microbands pre-screened with in situ analysis. Chem. Geol. 285, 133–143.

Becq-Giraudon, J.-F., Bouillé, S., Chauvel, J.-J., 1992. Genesis and significance of the silico-aluminous nodules in the Ordovician of the Montagne Noire and the Massif Armoricain (France). Sediment. Geol. 77, 77–87.

Bustillo, M.A., Castaneda, N., Capote, M., Consuegra, S., Criado, C., Diaz-Del-Rio, P., Orozco, T., Perez-Jimenez, J.L., Terradas, X., 2009. Is the macroscopic classification of flint useful? A petroarchaeological analysis and characterization of flint raw materials from the Iberian Neolithic mine of Casa Montero. Archaeometry 51, 175–196.

Cackler, P.R., Glascock, M.D., Neff, H., Iceland, H., Pyburn, K.A., Hudler, D., Hester, T.R., Chiarulli, B.M., 1999. Chipped stone artefacts, source areas, and provenance studies of the Northern Belize chert-bearing zone. J. Archaeol. Sci. 26, 389–397.

Calegari, G., 1993. Le perle in «corniola» di Taouardei (Mali). Mem. Soc. Ital. Sci. Nat. Mus. Civ. Stor. Nat. Milano 26, 117–120.

Caucia, F., Marinoni, L., Bordoni, V., Ghisoli, C., Adamo, I., 2012. Physical and chemical properties of some Italian opals. Period. Mineral. 81, 93–106.

Cifani, G., Munzi, M., 2003. Alle sorgenti del Cinyps. Libyan Stud. 34, 85–100.

Chang, H.J., Chu, X.L., Feng, L.J., Huang, J., 2009. Terminal Ediacaran anoxia in deep-ocean: trace element evidence from cherts of the Liuchapo Formation, South China. Sci. China, Ser. Earth Sci. 52, 807–822.

Cole, F., 2013. Small finds reports. In: Mattingly, D.J. (Ed.), The Archaeology of Fazzān, Survey and Excavations at Old Jarma (Ancient Garama) Carried Out by C.M. Daniels (1962–69) and the Fazzān Project (1997–2001), vol. 4. Society for Libyan Studies, Department of Antiquities, London, pp. 455–472.

Craddock, P.T., Cowell, M.R., Leese, M.N., Hughes, M.J., 1983. The trace element composition of polished flint axes as an indicator of source. Archaeometry 25, 135–163.

De Bruin, M., Korthoven, P.J.M., Bakels, C.C., Groen, F.C.A., 1972. The use of non-destructive activation analysis and pattern recognition in the study of flint artefacts. Archaeometry 14, 55–63.

De Michele, V., Piacenza, B., 1999. L'amazzonite di Eghei Zuma (Tibesti settentrionale, Libia). Sahara 11, 109–111.

Denham, D., Clapperton, H., 1826. Narration of Travels and Discoveries in Northern and Central Africa in the Years 1822–1824. John Murray, London.

Desanges, J., 1980. (Pliné l'Ancien), Histoire Naturelle, Livre V,1-46 (L'Afrique du Nord). Paris.

Di Leo, P., Dinelli, E., Mongelli, G., Schiattarella, M., 2002. Geology and geochemistry of Jurassic pelagic sediments, Scisti silicei Formation, southern Apennines, Italy. Sediment. Geol. 150, 229–246.

Eker, C.S., Sipahi, F., Kaygusuz, A., 2012. Trace and rare earth elements as indicators of provenance and depositional environments of Lias cherts in Gumushane, NE Turkey. Chem. Erde 72, 167–177.

Evans, A.A., Donahue, R.E., 2005. The elemental chemistry of lithic microwear: an experiment. J. Archaeol. Sci. 32, 1733–1740.

Evans, A.A., Wolframm, Y.B., Donahue, R.E., Lovis, W.A., 2007. A pilot study of "black chert" sourcing and implications for assessing hunter–gatherer mobility strategies in Northern England. J. Archaeol. Sci. 34, 2161–2169.

Francis Jr., P., 2002. Asia's Maritime Bead Trade: 300 BC to the Present. University of Hawaii Press, Honolulu.

Gaillou, E., Delaunay, A., Rondeau, B., Bouhnikle-Coz, M., Fritsch, E., Cornen, G., Monnier, C., 2008. The geochemistry of gem opals as evidence of their origin. Ore Geol. Rev. 34, 113–126.

Glascock, M.D., 2004. Neutron activation analysis of chert artifacts from a Hopewell mound. J. Radioanal. Nucl. Chem. 262, 97–102.

Gliozzo, E., Grassi, N., Bonanni, P., Meneghini, C., Tomei, M.A., 2011. Gemstones from Vigna Barberini at the Palatine hill (Rome, Italy). Archaeometry 53, 469–489.

Gotze, J., Nasdala, L., Kleeberg, R., Wenzel, M., 1998. Occurrence and distribution of "moganite" in agate/chalcedony: a combined micro-Raman, Rietveld, and cathodoluminescence study. Contrib. Mineral. Petrol. 133, 96–105.

Götze, J., Tichomirowa, M., Fuchs, H., Pilot, J., Sharp, Z.D., 2001. Geochemistry of agates: a trace element and stable isotope study. Chem. Geol. 175, 523–541.

Götze, J., Möckel, R., Kempe, U., Kapitonov, I., Vennemann, T., 2009. Characteristics and origin of agates in sedimentary rocks from the Dryhead area, Montana, USA. Mineral. Mag. 73, 673–690.

Graetsch, H.A., Grünberg, J.M., 2012. Microstructure of flint and other chert raw materials. Archaeometry 54, 18–36.

Grenne, T., Slack, J.F., 2005. Geochemistry and jasper beds from the Ordovician Løkken ophiolite, Norway: origin of proximal and distal siliceous exhalites. Econ. Geol. 100, 1511–1527.

Guérin, G., Discamps, E., Lahaye, C., Mercier, N., Guibert, P., Turq, A., Dibble, H.L., McPherron, S.P., Sandgathe, D., Goldberg, P., Jain, M., Thomsen, K., Patou-Mathis, M., Castel, J.-C., Soulier, M.-C., 2012. Multi-method (TL and OSL), multi-material (quartz and flint) dating of the Mousterian site of Roc de Marsal (Dordogne, France): correlating Neanderthal occupations with the climatic variability of MIS 5–3. J. Archaeol. Sci. 39, 3071–3084.

Halamić, J., Marchig, V., Goričan, S., 2001. Geochemistry of triassic radiolarian cherts in North-Western Croatia. Geol. Carpath. 52, 327–342.

Hatipoğlu, M., Tuncer, Y., Kibar, R., Çetin, A., Karali, T., Can, N., 2010. Thermal properties of gem-quality moganite-rich blue chalcedony. Phys. B 405, 4627–4633.

Hatipoğlu, M., Ajò, D., Sezai Kırıkoğl, M., 2011a. Cathodoluminescence (CL) features of the Anatolian agates, hydrothermally deposited in different volcanic hosts from Turkey. J. Lumin. 131, 1131–1139.

Hatipoğlu, M., Oren, U., Kibici, Y., 2011b. Micro-Raman spectroscopy of gem-quality chrysoprase from the Biga–Canakkale region of Turkey. J. Afr. Earth Sci. 61, 273–285.

Heaney, P.J., 1995. Moganite as an indicator for vanished evaporites: a testament reborn? J. Sediment. Petrol. A65, 633–638.

Hess, S.C., 1996. Chert provenance analysis at the Mack Canyon site, Sherman County, Oregon: an evaluative study. Geoarchaeology 11, 51–81.

Huckell, B.B., Kilby, J.D., Boulanger, M.T., Glascock, M.D., 2011. Sentinel Butte: neutron activation analysis of White River group chert from a primary source and artifacts from a Clovis cache in North Dakota, USA. J. Archaeol. Sci. 38, 965–976.

Insoll, T., Polya, D.A., Bhan, K., Irving, D., Jarvis, K., 2004. Towards an understanding of the carnelian bead trade from Western India to sub-Saharan Africa: the application of UV-LA-ICP-MS to carnelian from Gujarat, India, and West Africa. J. Archaeol. Sci. 31, 1161–1173.

Karacik, Z., Genc, S.C., Esenli, F., Goller, G., 2011. The Gumuldur Fire Opal: mode of occurrence and mineralogical aspects. Turk. J. Earth Sci. 20, 99–114.

Kasztovszky, Z.S., Biró, K.T., Markó, A., Dobosi, V., 2008. Cold neutron prompt gamma activation analysis – a non-destructive method for characterization of high silica content chipped stone tools and raw materials. Archaeometry 50, 12–29.

Larson, A.C., Von Dreele, R.B., 1994. General Structure Analysis System (GSAS). Los Alamos National Laboratory Report LAUR 86–748.

Law, R., Carter, A., Bhan, K., Malik, A., Glascock, M.D., 2012. INAA of agate sources and artifacts from the Indus, Helmand, and Thailand regions. In: Frenez, D., Tosi, M. (Eds.), South Asian Archaeology 2007-Proceedings of the 19th International Conference of the European Association of South Asian Archaeology (Ravenna, Italy, 2–6 July 2007), British Archaeological Reports, International Series, vol. 2454, pp. 177–184.

Levtzion, N., Hopkins, J.F.P., 2000. Corpus of Early Arab Sources for West African History. Princeton University Press, Princeton.

Liégeois, J.P., Benhallou, A., Azzouni-Sekkal, A., Yahiaoui, R., Bonin, B., 2005. The Hoggar swell and volcanism: reactivation of the Precambrian Tuareg shield during Alpine convergence and West African Cenozoic volcanism. In: Foulger, G.R., Natland, J.H., Presnall, D.C., Anderson, D.L. (Eds.), Plates, Plumes and Paradigms, vol. 388. Geological Society of America, pp. 379–400. Special Paper.

Luedtke, B.E., 1978. Chert sources and trace-element analysis. Am. Antiq. 43, 413–423.

Lyons, W.H., Glascock, M.D., Mehringer Jr., P.J., 2003. Silica from sources to site: ultraviolet fluorescence and trace elements identify cherts from Lost Dune, southeastern Oregon, USA. J. Archaeol. Sci. 30, 1139–1159.

Machado, J., Hernández, C.M., Mallol, C., Galván, B., 2013. Lithic production, site formation and Middle Palaeolithic palimpsest analysis: in search of human occupation episodes at Abric del Pastor Stratigraphic Unit IV (Alicante, Spain). J. Archaeol. Sci. 40, 2254–2273.

Manetti, P., Peccerillo, A., Poli, G., 1979. Rare earth element distribution in Jurassic siliceous rocks from northern Apennines (Italy). Mineral. Petrogr. Acta 23, 87–98.

Marcoux, E., Le Berre, P., Cocherie, A., 2004. The Meillers Autunian hydrothermal chalcedony: first evidence of a similar to 295 Ma auriferous epithermal sinter in the French Massif Central,. Ore Geol. Rev. 25, 69–87.

Mattingly, D.J. (Ed.), 2003. The Archaeology of Fazzān. Synthesis, vol. 1. Society for Libyan Studies, Department of Antiquities, London.

Mattingly, D.J. (Ed.), 2007. The Archaeology of Fazzān. Site Gazetteer, Pottery and Other Survey Finds, vol. 2. Society for Libyan Studies, Department of Antiquities, London.

Mattingly, D.J., 2010. The Archaeology of Fazzān. Excavations Carried Out by C. M. Daniels, vol. 3. Society for Libyan Studies, Department of Antiquities, London.

Mattingly, D.J. (Ed.), 2013. The Archaeology of Fazzān. Survey and Excavations at Old Jarma (Ancient Garama) Carried Out by C.M. Daniels (1962–69) and the Fazzān Project (1997–2001), vol. 4. Society for Libyan Studies, Department of Antiquities, London.

Mercier, N., Valladas, H., Falguères, C., Shao, Q., Gopher, A., Barkai, R., Bahain, J.-J., Vialettes, L., Joron, J.-L., Reyss, J.-L., 2013. New datings of Amudian layers at Qesem Cave (Israel): results of TL applied to burnt flints and ESR/U-series to teeth. J. Archaeol. Sci. 40, 3011–3020.

Miehe, G., Graetsch, H., 1992. Crystal structure of moganite: a new structure type of silica. Eur. J. Mineral. 4, 693–706.

Migaszewski, Z.M., Gałuszka, A., Durakiewicz, T., Starnawska, E., 2006. Middle Oxfordian-lower Kimmeridgian chert nodules in the Holy Cross mountains, south-central Poland. Sediment. Geol. 187, 11–28.

Misik, M., 1996. Silica spherulites and fossil silcretes in carbonate rocks of the Western Carpathians. Geol. Carpath. 47, 91–105.

Möckel, R., Götze, J., Sergeev, S.A., Kapitonov, I.N., Adamskaya, E.V., Goltsin, N.A., Vennemann, T., 2009. Trace-element analysis by laser ablation inductively coupled plasma mass spectrometry (LA-ICP-MS): a case study for agates from Nowy Kościoł, Poland. J. Sib. Fed. Univ. Eng. Technol. 2, 123–138.

Monod, T., 1984. L'emeraude des Garamantes. Souvenirs d'un Saharien. Paris.
Murray, R.W., Buchholtz Ten Brink, M.R., Gerlach, D.C., Price Russ II, G., Jones, D.L., 1991. Rare earth, and trace elements in chert from the Franciscan Complex and Monterey Group, California: assessing REE sources to fine-grained marine sediments. Geochim. Cosmochim. Acta 55, 1875–1895.
Murray, R.W., Buchholtz Ten Brink, M.R., Gerlach, D.C., Price Russ II, G., Jones, D.L., 1992. Rare earth, major and trace element composition of Monterey and DSDP chert and associated host sediment: assessing the influence of chemical fractionation during diagenesis. Geochim. Cosmochim. Acta 56, 2657–2671.
Nathan, Y., Segal, I., Delage, C., 1999. Geochemical characterization of cherts from northern Israel (western Galilee). Isr. J. Earth Sci. 48, 235–245.
Navazo, M., Colina, A., Domínguez-Bella, A., Benito-Calvo, A., 2008. Raw stone material supply for Upper Pleistocene settlements in Sierra de Atapuerca (Burgos, Spain): flint characterization using petrographic and geochemical techniques. J. Archaeol. Sci. 35, 1961–1973.
Olofsson, A., Rodushkin, I., 2011. Provenancing flint artefacts with ICP–MS using REE signatures and Pb isotopes as discriminants: preliminary results of a case study from northern Sweden. Archaeometry 53, 1142–1170.
Parali, L., Garcia Guinea, J., Kibar, R., Cetin, A., Can, N., 2011. Luminescence behaviour and Raman characterization of dendritic agate in the Dereyalak village (Eskişehir), Turkey. J. Lumin. 131, 2317–2324.
Peng, Jun, Yi, H., Xia, W., 2000. Geochemical criteria of the Upper Sinian cherts of hydrothermal origin on the southeast continental margin of the Yangtze Plate. Chin. J. Geochem. 19, 217–226.
Pettitt, P., Rockman, M., Chenery, S., 2012. The British Final Magdalenian: society, settlement and raw material movements revealed through LA-ICP-MS trace element analysis of diagnostic artefacts. Quat. Int. 272–273, 275–287.
Pitblado, B.L., Cannon, M.B., Neff, H., Dehler, C.M., Nelson, S.T., 2013. LA-ICP-MS analysis of quartzite from the Upper Gunnison Basin, Colorado. J. Archaeol. Sci. 40, 2196–2216.
Pretola, J.P., 2001. A feasibility study using silica polymorph ratios for sourcing chert and chalcedony lithic materials. J. Archaeol. Sci. 28, 721–739.
Rapp, G.R., 2002. Archaeomineralogy. Springer-Verlag, Berlin.
Rohlfs, G., 2001. Voyages et explorations au Sahara. Il Tripoli – Rhadames – Fezzan – Kaouar – Bornou 1865–67. Karthala, Paris.
Rosenfeld, A., Dvorachek, M., Amorai-Stark, S., 2003. Roman wheel-cut engraving, dyeing and painting microquartz gemstones. J. Archaeol. Sci. 30, 227–238.
Sax, M., Meeks, N.D., 1995. Methods of engraving Mesopotamian quartz cylinder seals. Archaeometry 37, 25–36.
Sax, M., Mcnabb, J., Meeks, N.D., 1998. Methods of engraving Mesopotamian cylinder seals: experimental confirmation. Archaeometry 40, 1–21.
Schmidt, C., Pettke, T., Preusser, F., Rufer, D., Uwe Kasper, H., Hilgers, A., 2012a. Quantification and spatial distribution of dose rate relevant elements in silex used for luminescence dating. Quat. Geochronol. 12, 65–73.
Schmidt, P., Léa, V., Sciau, Ph, Fröhlich, F., 2012b. Detecting and quantifying heat treatment of flint and other silica rocks: a new non-destructive method applied to heat-treated flint from the Neolithic Chassey culture, southern France. Archaeometry 55, 794–805.
Schmidt, C., Rufer, D., Preusser, F., Krbetschek, M., Hilgers, A., 2013a. The assessment of radionuclide distribution in silex by autoradiography in the context of dose rate determination for thermoluminescence dating. Archaeometry 55, 407–442.
Schmidt, P., Porraz, G., Slodczyk, A., Bellot-gurlet, L., Archer, W., Miller, C.E., 2013b. Heat treatment in the South African Middle Stone Age: temperature induced transformations of silcrete and their technological implications. J. Archaeol. Sci. 40, 3519–3531.
Schmidt, P., Bellot-Gurlet, L., Léa, V., Sciau, P., 2013c. Moganite detection in silica rocks using Raman and infrared spectroscopy. Eur. J. Mineral. 25, 797–805.
Simoni, M., Caucia, F., Adamo, I., Galinetto, P., 2010. New occurrence of fire opal from Bemia, Madagascar. Gems Gemol. 46 (2), 114–121.
Stemp, W.J., Childs, B.E., Vionnet, S., Brown, C.A., 2009. Quantification and discrimination of lithic use-wear: surface profile measurements and length-scale fractal analysis. Archaeometry 51, 366–382.
ten Bruggencate, R.E., Fayek, M., Brownlee, K., Brooke Milne, S., Hamilton, S., 2013. A combined visual-geochemical approach to establishing provenance for pegmatite quartz artifacts. J. Archaeol. Sci. 40, 2702–2712.
Tiepolo, M., Bottazzi, P., Palenzona, M., Vannucci, R., 2003. A laser probe coupled with ICP-double focusing sector-field mass spectrometer for in situ analysis of geological samples and U-Pb dating of zircon. Can. Mineral. 41, 259–272.
Toraya, H., 2000. Estimation of statistical uncertainties in quantitative phase analysis using the Rietveld method and the whole-powder-pattern decomposition method. J. Appl. Crystallogr. 33, 1324–1328.
Tsobgou, R.A., 2009. Mapping Mesolithic and Neolithic cultures behaviours and interactions with nature and properties of rocks in Western France. J. Archaeol. Sci. 36, 1615–1625.
van Achterbergh, E., Ryan, C.G., Jackson, S.E., Griffin, W.L., 2001. Data reduction software for LA-ICP-MS. In: Sylvester, P. (Ed.), Laser-ablation-ICPMS in the Earth Sciences: Principles and Applications, vol. 29. Minereralogical Association of Canada, pp. 239–243.
Zerboni, A., Vignola, P., 2013. Greenstone beads from the excavation in Fewet. In: Mori, L. (Ed.), Life and death of arural village in Garamantian Times. Archaeological investigations in the Fewet oasis (Libyan Sahara). Arid Zone Archaeology Monographs, 6. Edizioni all'Insegna del Giglio, Firenze, pp. 157–167.
Wang, J., Chen, D., Wang, D., Yan, D., Zhou, X., Wang, Q., 2012. Petrology and geochemistry of chert on the marginal zone of Yangtze Platform, western Hunan, South China, during the Ediacaran–Cambrian transitino. Sedimentology 59, 809–829.
Yonekura, K., Hasegawa, H., Hotta, A., Suzuki, T., 2008. A novel approach to studies of prehistoric exploitation of stone tool materials using material composition, surface morphology, microstructure and mechanical properties. Archaeometry 50, 727–746.